

# TECHNICAL NOTE

D-1022

A STUDY OF THE AERODYNAMIC CHARACTERISTICS OF  
A FIXED GEOMETRY PARAGLIDER CONFIGURATION AND  
THREE CANOPIES WITH SIMULATED VARIABLE CANOPY  
INFLATION AT A MACH NUMBER OF 6.6

By Jim A. Penland

Langley Research Center  
Langley Air Force Base, Va.

NATIONAL AERONAUTICS AND SPACE ADMINISTRATION  
WASHINGTON

March 1962



## NATIONAL AERONAUTICS AND SPACE ADMINISTRATION

## TECHNICAL NOTE D-1022

A STUDY OF THE AERODYNAMIC CHARACTERISTICS OF  
A FIXED GEOMETRY PARAGLIDER CONFIGURATION AND  
THREE CANOPIES WITH SIMULATED VARIABLE CANOPY  
INFLATION AT A MACH NUMBER OF 6.6

By Jim A. Penland

## SUMMARY

Three-component force tests have been made at a Mach number of 6.6 and a Reynolds number of  $0.24 \times 10^6$  based on the keel length of a fixed-geometry paraglider configuration consisting of a canopy made from two conical steel shells joined along a common keel line and having leading-edge and shroud-line diameters of 1.8 percent of the keel length and a payload diameter of 11 percent of the keel length. Further force tests were made on unshrouded canopies with three different degrees of simulated canopy inflation. Oil-flow and temperature-sensitive-paint tests were made to study the effects of canopy geometry and shroud interference on local flow fields and aerodynamic heating. Measured force characteristics are compared with Newtonian theory, which was generally found to underpredict the magnitude of the parameters on the models having concave lower surfaces. The addition of shrouds and payload reduced the maximum lift-drag ratio of the canopy from 1.53 to 1.05. Indications from oil-flow and temperature-sensitive-paint tests are that severe and extensive regions of aerodynamic heating on the canopy (as compared with the heating on the nose) are encountered on configurations of this type.

## INTRODUCTION

Much interest has been shown in making use of paraglider devices during the reentry of orbital vehicles, in the recovery of expended launch-vehicle casings, and as auxiliary high-lift devices for aircraft (refs. 1 to 4). Even though the current major effort is in the development of the concept for use at subsonic and low supersonic speeds at the end of an orbital or suborbital flight, other possible applications for the concept exist for crew and payload recovery at higher speeds in

the trajectory. Such a contrivance would fulfill the need for a controllable and equally storable replacement for the parachute and would provide both lift and lift-drag ratios greater than zero.

The purpose of this investigation was (1) to determine experimentally and theoretically the static longitudinal characteristics at hypersonic speeds of a complete paraglider vehicle and three canopy configurations with various degrees of simulated canopy inflation, (2) to determine by oil-flow technique the surface flow direction and the regions of high shear, and (3) to locate regions of high aerodynamic heating by using temperature-sensitive paint.

For practical considerations the models were constructed of solid material and are therefore of fixed geometry. The information gained on the complete paraglider model provides a basis for comparison of such non-rigid configurations because of its aerodynamic cleanness and absence of ripples, porosity, and flutter. The parawing models with various degrees of canopy inflation provide an insight into the effects of changing leading-edge sweep, wing span, and camber on the static longitudinal characteristics of flexible parawing configurations as well as extend the general delta-wing program to include lower surface concavity in the form of two semiconical lobes.

#### SYMBOLS

$C_A$	axial-force coefficient, $F_A/q_\infty S$
$C_D$	drag coefficient, $F_D/q_\infty S$
$C_L$	lift coefficient, $F_L/q_\infty S$
$C_m$	pitching-moment coefficient, $M_Y/q_\infty S \bar{c}$
$C_N$	normal-force coefficient, $F_N/q_\infty S$
$C_{p,i}$	local pressure coefficient
$\bar{c}$	reference length, 69 percent of theoretical model length
$F_A$	axial force
$F_D = F_N \sin \alpha + F_A \cos \alpha$	

L  
1  
8  
4  
9

$$F_L = F_N \cos \alpha - F_A \sin \alpha$$

$F_N$  normal force

$L/D$  lift-drag ratio,  $C_L/C_D$

$M_Y$  pitching moment

$M_\infty$  free-stream Mach number

$q_\infty$  free-stream dynamic pressure

$R_\infty$  free-stream Reynolds number, based on body length

$S$  planform area of model in the flat or uninflated condition

$X, Y, Z$  body axes

$\alpha$  angle of attack of models, measured between model keel and airflow, deg

$\alpha_c$  angle of attack of theoretical cone, measured in the X-Z body plane, deg

$\alpha'$  pitch angle of theoretical cone, measured in the X-Z wind plane, deg

$\beta_c$  angle of sideslip of theoretical cone, measured in the X-Y wind plane, deg

$\beta'$  yaw angle of theoretical cone, measured in the X-Y body plane, deg

$\delta$  local flow deflection angle, deg

$\eta$  angle between the local normal vector and the free-stream velocity vector, deg

$\theta_c$  semivertex angle of theoretical cone, deg

$\phi$  angular position of local element on surface of theoretical cone, deg

L  
1  
8  
4  
9

## APPARATUS AND TESTS

The tests were conducted in the Mach number 6.86 test section of the Langley 11-inch hypersonic tunnel. The tunnel-wall boundary-layer thickness and hence the free-stream Mach number of this test section are dependent upon the stagnation pressure. For these tests, at an average stagnation pressure of 5 atmospheres and an average stagnation temperature of 560° F (to avoid liquefaction), the average free-stream Mach number was 6.6 and the average Reynolds number was  $0.675 \times 10^5$  per inch. The absolute humidity was kept to less than  $1.9 \times 10^{-5}$  pounds of water per pound of dry air for all tests. Three-component force data were obtained by use of a strain-gage force balance through an angle-of-attack range of about 10° to 75° at zero angle of sideslip.

L  
1  
8  
4  
9

Oil-flow studies were conducted by applying dots of an oil-lampblack mixture approximately 1/8 inch apart on the surface of the stainless-steel force models and exposing the model for a short time to the free-stream flow. For these tests, the desired tunnel air temperature was attained by bypassing air around the test section; at time zero the bypass valve was closed, and the valve to the tunnel nozzle was opened to provide an approximately instantaneous start of hypersonic flow through the test section. The models were observed visually, and the flow was shut off about 4 seconds after time zero. No significant changes of the oil-flow pattern were observed as a result of shutting off the tunnel flow.

Temperature-sensitive-paint studies were conducted by spraying the paint on fiber-glass models and exposing them to the free-stream flow in a manner identical to that described previously for the oil-flow tests.

## MODELS

Photographs of the force models used in the present investigation are shown in figure 1 and the detail drawings are shown in figures 2 and 3. These models were made of stainless steel and consisted of a complete paraglider configuration and three paraglider canopies with various degrees of simulated canopy inflation. When uninflated all three canopies had common planforms like the 0° canopy. The model design was based on a full-scale configuration which had a keel length of 100 feet and 2-foot-diameter inflatable leading edges and shrouds to alleviate aerodynamic heating. Inasmuch as the canopy inflation or shape is a function of several variables (including the aerodynamic

loading and the method of rigging), three models were designed to study the effects of span and leading-edge-sweep changes.

The 100° canopy and the 180° canopy were generated by assuming that inflation would give a conical form; thus, the 100° canopy was composed of two 100° segments of a theoretical cone having a semivertex angle of 26.77° and the 180° canopy was made up of two 180° segments of a theoretical cone having a semivertex angle of 14.10°. The schematic drawings of figure 3 illustrate this design method. The two conical segments were welded together along the keel to complete each configuration. The three models provide changes in leading-edge sweep of 45°, 49.64°, and 61.8°.

The complete model was a combination of the 180° canopy with steel rods and a steel sphere silver soldered in place to simulate shrouds and payload, respectively. Each model had two adapters to make possible tests at angles of attack of approximately 10° to 75° while rotating the strut and balance through an angle-of-attack range of -5° to 30°. The 180° canopy and the complete configuration were also used for the oil-flow study.

The models used for the temperature-sensitive-paint investigation were constructed of white fiber glass and were scaled-up versions of the 180° canopy model, the complete configuration, and the nose portion of the complete configuration, respectively, as shown in figure 4. Metal inserts needed for structural strength were well submerged beneath the surface of the fiber-glass material to minimize the effects of conduction.

#### THEORETICAL CALCULATIONS

The aerodynamic force and moment characteristics of the models at hypersonic speeds were calculated throughout the angle-of-attack range from 0° to 90°, and the results are presented along with the experimental data.

The calculations were made by using the Newtonian theory (ref. 5) which presents the relation

$$C_{p,l} = 2 \sin^2 \delta$$

where  $\delta$  is the local flow deflection angle. The local flow deflection angles were found by using equation (5) of reference 6 which is

$$\begin{aligned} \cos \eta = & \sin \theta_c \cos \alpha_c \cos \beta_c - \cos \theta_c \sin \phi \sin \beta_c \\ & - \cos \theta_c \cos \phi \sin \alpha_c \cos \beta_c \end{aligned}$$

and the following relations between the geometry of the theoretical cones (shown as dashed lines in fig. 3) and their orientation with respect to the airstream:

$$\sin \alpha_c = \frac{\sin \alpha'}{\cos \beta_c}$$

$$\sin \beta_c = \cos \alpha' \sin \beta'$$

The relation between  $\alpha$  and  $\alpha'$  is as follows:

$$\alpha' = \alpha + 16.82^\circ \quad (100^\circ \text{ canopy})$$

$$\alpha' = \alpha \quad (180^\circ \text{ canopy})$$

The angle  $\eta$  is the angle between the free-stream velocity vector and the local normal vector and is therefore equal to  $90^\circ$  when the flow is perpendicular to the local normal vector and the local flow deflection angle equals  $0^\circ$ . When the value of  $\eta$  is greater than  $90^\circ$ , the concave lower surface of the model is exposed to the free-stream flow and the local flow deflection given by the relation  $\delta = \eta - 90^\circ$ .

The local pressure coefficients may therefore be determined from the relation  $C_{p,l} = 2 \sin^2(\eta - 90^\circ)$ . The concave surfaces were divided into a number of triangular elements, the local pressure coefficients were determined as outlined previously, and the total force coefficients were determined by a numerical integration of these local pressure coefficients. The pitching moment was determined by summing the local normal- and axial-force coefficients for each of the small elements of the canopies and for each leading edge, shroud, and payload multiplied by its individual moment arm. Leading edges and shrouds were assumed to be circular cylinders at combined angles of attack and sideslip, and the payload was assumed to be a sphere. No estimates of skin friction were included in the calculations.

#### ACCURACY OF MEASUREMENT

The maximum uncertainties in the measurement of the force and moment coefficients for the individual test points as a result of the force balance system computed by formulas derived from the method of least squares (ref. 7) are presented as follows:

$C_L$ . . . . .	$\pm 0.04$
$C_D$ . . . . .	$\pm 0.04$
$C_N$ . . . . .	$\pm 0.04$
$C_A$ . . . . .	$\pm 0.02$
$C_m$ . . . . .	$\pm 0.03$

## PRESENTATION OF RESULTS

The force and moment coefficients are referred to the wind- and body-axis system. The data for the various canopies and the complete paraglider configuration are presented separately. The longitudinal characteristics of the three canopies are presented first along with calculations made by the Newtonian theory. The characteristics of the complete paraglider configuration are then presented along with theoretical results. A study of the effects of adding the shrouds and payload to the canopy was conducted by use of schlieren photographs, oil flow, and temperature-sensitive paint. The figures are presented as follows:

	Figure
Effect of the degree of canopy inflation on longitudinal characteristics of paraglider canopy . . . . .	5
Schlieren photographs of various canopies . . . . .	6
Comparison of longitudinal characteristics of three canopies of various degrees of canopy inflation with Newtonian theory . . . . .	7
Comparison of lift-drag ratios and lift coefficients of various canopies . . . . .	8
Effect of addition of shrouds and payload on longitudinal characteristics of $180^\circ$ canopy . . . . .	9
Comparison of longitudinal characteristics of complete paraglider configuration with Newtonian theory . . . . .	10
Comparison of photographs of schlieren, oil flow, and temperature-sensitive-paint investigations of $180^\circ$ canopy configuration at various angles of attack . . . . .	11
Comparison of photographs of schlieren, oil flow, and temperature-sensitive-paint investigations of the complete paraglider configuration at various angles of attack . . . . .	12
Effect of Reynolds number on aerodynamic heating characteristics of complete paraglider configuration in vicinity of leading-edge—shroud intersection obtained by use of temperature-sensitive paint . . . . .	13

## RESULTS AND DISCUSSION

Inasmuch as the primary purpose of this study was to investigate the flexible paraglider concept, the basic uninflated projected area was used for reference in the presentation and analysis of theory and data. For those who prefer the planform area of each individual configuration as reference, the following table of ratios is provided for convenient conversion of presented data:

Configuration	$\frac{\text{Uninflated area}}{\text{Inflated area}}$
0° canopy . . . . .	1.000
100° canopy . . . . .	1.128
180° canopy . . . . .	1.636
Complete paraglider . . . . .	1.636

L  
1  
8  
4  
9

## Various Paraglider Canopies

Effect of canopy inflation.- A comparison of the experimental longitudinal characteristics of the three canopies is presented in figures 5(a) and 5(b). These data show that all three models have similar trends with angle of attack for any given coefficient and that the effect of increasing the canopy inflation or the lower surface concavity appears mainly as a decrease in the magnitude of the coefficients, and a displacement of the maximum and minimum values with respect to the angle of attack. Although there was a general decrease in the lift and drag coefficients with increasing canopy inflation, the corresponding decrease in drag was proportionally greater giving a net increase of lift-drag ratio for the 100° and 180° canopy models at angles of attack above those for the maximum lift-drag ratio. The angle of attack where both the maximum lift and the maximum lift-drag ratio occurred increased with inflation. This increase in the ratio of lift to drag is due in part to the negative increase of the axial force with canopy inflation which contributed to the configuration lift while tending to decrease the drag. Normal force decreased considerably due partly to the decrease in projected area with canopy inflation. For the particular center-of-gravity location chosen, the stability appeared to increase with inflation although there was considerable scatter in the data, most of which was within the accuracy of measurement.

Schlieren photographs.- Figure 6 shows schlieren photographs of the three canopies at about 15° intervals throughout the angle-of-attack range of the tests. At an angle of attack of 15°, each photograph shows that the balance adapter attached to the top of each canopy was exposed

to the expanded flow in that region. These shocks caused by the adapters were visible only at angles of attack below about  $25^\circ$ , and therefore only those data were affected by the resulting slight increase in axial force and by the decrease in normal force due to these disturbances. Because of the rearward location of the adapters and their proximity to the center of gravity, only the adapter axial force would contribute measurably to the pitching moment and this would occur only at low angles of attack. Of particular interest is the location of the bow shock wave in relation to the models. This detached shock wave is pulled in closer to the lower surface elements of the model with increasing inflation for all angles of attack to such an extent that the maximum distance between the shock wave and the lower surface of the model is little different from the distance between the shock wave and the lower surface of the flat plate. This means that a large portion of the lower concave surface is closer to the shock wave than in the case of the flat plate, and inasmuch as the surface pressure is a function of the shock-to-surface distance, higher local pressures are to be expected than on corresponding portions of the  $0^\circ$  canopy or flat-plate model.

Data and theory for canopies.- A comparison of the longitudinal characteristics of the three canopies with calculations made by using the Newtonian theory is presented in figures 7(a) to 7(f). As expected, the Newtonian or impact theory gave excellent predictions of the trends of the longitudinal force and moment characteristics with angle of attack but failed to give the magnitude of the individual coefficients adequately. This difference was due to the presence of several shocks from the leading edges and keel and the effects of their interaction on the canopy surface pressure forces which are not accounted for by the Newtonian theory.

Generally the theory underpredicted the experimental values throughout the angle-of-attack range, and with the exception of pitching moment and lift-drag ratio, the discrepancy between experiment and theory increased with increasing lower surface concavity or inflation. The angle of attack where the maximum lift occurred increased with inflation; this trend was predicted by the calculations (fig. 7(a)). Both the value of the maximum  $L/D$  for all canopies and the angles of attack where the maximums occurred were well predicted (fig. 7(c)). The estimates of the pitching moment (fig. 7(d)) were good in the stable region below an angle of attack of about  $50^\circ$ , but the unstable or neutrally stable region at the higher angles of attack was not predicted. The underprediction of the normal-force coefficients (fig. 7(e)) for the  $100^\circ$  and  $180^\circ$  canopies was considerably greater than for the  $0^\circ$  canopy or flat-plate model, an indication, as discussed in the section entitled "Schlieren photographs," that the local pressure coefficients inside the concave surfaces are higher than those on a flat plate oriented at the same local angle to the flow. This conjecture was

verified by a comparison of measured pressures on a similar configuration taken at  $M_\infty = 4.65$  (unpublished results obtained in the Langley Unitary Plan wind tunnel) with the calculated local pressures on the  $180^\circ$  canopy. The axial force (fig. 7(f)) on the flat-plate model was well predicted and was made up of only the leading edge and nose forces. The trend of a negative axial force on the  $100^\circ$  and  $180^\circ$  canopies which increases with angle of attack was given by the calculations, although again the magnitude of the experimental data was considerably in excess of the predicted values. A few tests were made on the three canopies at a Reynolds number of  $0.48 \times 10^6$  and the lift-drag ratio results are shown in figure 7(c) by flagged symbols. This figure shows that the increase in Reynolds number by a factor of two had little effect on the lift-drag ratio, a parameter which is usually sensitive to small changes in force characteristics; thus, it may be concluded that the effect of Reynolds number on the measured forces was small.

L  
1  
8  
4  
9

During reentry the lift and the lift-drag ratio of a configuration markedly affect the allowable entry angle, the deceleration, and the total heat load of the vehicle; it is therefore desirable to compare these parameters for the various canopies (fig. 8). This comparison shows that both the experimental and calculated maximum lift-drag ratios for all canopies occur at approximately the same value of constant lift coefficient; furthermore, the maximum lift coefficient for each model occurs at approximately the same lift-drag ratio. As already pointed out, the maximum lift-drag ratio decreases with increasing canopy inflation; however, the maximum lift decreases much more gradually with no decrease noted between the flat plate and the moderately inflated  $100^\circ$  canopy. With a wide range of lift coefficients and high lift-drag ratios being desirable for a reentry configuration, it appears that a large degree of inflation may be undesirable and that controlled inflation made possible by improved canopy design and rigging is highly desirable on flexible configurations.

### Complete Paraglider Configuration

Effect of addition of shrouds and payload to  $180^\circ$  canopy.- The addition of the six shrouds and the spherical payload to the  $180^\circ$  canopy had a significant effect on the aerodynamic-force characteristics (fig. 9). These additions resulted in an increase in the magnitude of normal force throughout the angle-of-attack range, an increase in the axial force in a positive direction up to about  $55^\circ$ , and a slight increase negatively at the higher angles of attack. As expected, this combination of normal and axial forces resulted in a net increase in drag throughout the angle-of-attack range and also an increase in the lift above an angle of attack of  $25^\circ$ . Although the maximum lift increased, the angle of attack where it occurred remained essentially constant at about  $67^\circ$ . The maximum

lift-drag ratio of the canopy alone was decreased from about 1.53 to about 1.05 for the complete configuration, and the angle of attack at which it occurred increased from about  $37^{\circ}$  to about  $52^{\circ}$ .

These effects which combine the pressure forces of the various components and the component interference are a direct function of the diameter, the length, and the geometric orientation of the shrouds and the payload, and it would therefore be expected that the aerodynamic characteristics would change significantly with any configuration change. Because of the lack of a common practical moment reference for the two configurations, no comparison was made of the pitching-moment characteristics.

Data and theory for paraglider.- A comparison of the basic longitudinal characteristics of the complete paraglider configuration with calculations made by using the Newtonian theory is presented in figure 10. The trends of both theory and experimental data for the complete paraglider are very similar to those previously shown for the  $180^{\circ}$  canopy; however, the discrepancy between theory and experiment is considerably greater for the complete configuration. The experimental coefficients were underestimated throughout most of the angle-of-attack range. Inasmuch as excellent predictions of lift-drag ratio were made on the  $180^{\circ}$  canopy, it would be expected that similar calculations on the complete configuration would be no less accurate; however, as mentioned previously, the addition of the shrouds and payload to the  $180^{\circ}$  canopy resulted in an increase in both lift and drag coefficients over those of the basic canopy. Comparisons of theoretical predictions for the  $180^{\circ}$  canopy and complete configuration (figs. 7 and 9, respectively) indicate that these increases were not predicted by theory; consequently, a considerably higher maximum lift-drag ratio was experimentally obtained for the complete configuration than that theoretically predicted. This difference was due in part to the flow interference of the shrouds and payload on the canopy pressure distribution. Such flow interference usually results in an increase in local pressure and this increase is somewhat substantiated by the fact that the difference between the experimental normal and axial coefficients and the theory, in which interference effects were not considered, was greater than the corresponding difference for the  $180^{\circ}$  canopy (fig. 7). Both the oil-flow and temperature-sensitive-paint tests, which will be discussed subsequently, indicate that the flow interference, and hence the increase in local pressures, were most noticeable on the downstream portion of the canopy. This observation would account for the increase in the experimental values of longitudinal stability over the predicted values.

### Flow Study

Technique.- From schlieren photographs the major flow disturbances, that is, shock and expansion waves, and their location with respect to

the model can be determined, and in the case of a complex configuration some regions of interference of one component on another may be ascertained. Oil-flow tests are restricted to surface flow conditions and can be used in determining the flow direction and regions of high shear due to variations of dynamic pressure, shock impingement, or boundary-layer variations. The use of temperature-sensitive paint gives indications of the location of regions or spots which are exposed to high temperature and thus show where the aerodynamic heating rate is greatest. By combining the three techniques on the same model under similar flow conditions at the same angle of attack, a reasonably good understanding of the flow may be obtained. A further understanding, in addition to that gained from the force and moment measurements, as to the effects of adding shrouds and a spherical payload to the  $180^\circ$  canopy was obtained by making oil-flow and temperature-sensitive-paint tests on both the  $180^\circ$  canopy and the complete paraglider configuration. A comparison of the results of using the three methods of flow study is presented in figure 11 for the  $180^\circ$  canopy and in figure 12 for the complete configuration at  $15^\circ$  increments through the test angle-of-attack range. The study series is complete except that no photographs for the temperature-sensitive-paint tests were available for  $\alpha = 15^\circ$ .

Flow variation with angle of attack for the  $180^\circ$  canopy.- The overall effects as seen in the schlieren photographs of increasing the angle of attack from  $15^\circ$  to  $75^\circ$  on the  $180^\circ$  canopy (fig. 11) were to shift the upper surface shock wave away from the model and shield the balance adapter from the flow, to force the lower surface shock wave closer to the model, and to expose the lower concave surface to the flow behind the bow shock. The oil-flow photographs show that there was a line of high shear on the inside of the lower concave surfaces near and parallel to the center ridge line at  $\alpha = 15^\circ$  in addition to a complete washing away of the oil on the leading-edge and nose regions. The shear line moved outboard with angle of attack and at  $\alpha = 75^\circ$  was submerged in the flow near the leading edges. The direction of the oil traces indicated that there was an outflow from the line of high shear at all angles of attack. At  $\alpha = 75^\circ$  the entire lower surface flow was nearly parallel to the stream, and with the exception of the leading edges there were no indications of regions of exceptionally high shear. There were indications of flow on the balance adapter (schlieren photograph) at  $\alpha = 15^\circ$  but none for the higher angles of attack. A definite upwash was indicated by the oil flow on the outside of the  $180^\circ$  canopy behind the leading edges. The temperature-sensitive-paint tests gave results that were similar to those found by using the oil-flow technique and showed that the leading edges and the line of shear were also the regions exposed to high aerodynamic heating compared with the heating rate on the nose. At  $\alpha = 75^\circ$  the entire lower concave surface showed the effects of a high heating rate only slightly less than the leading edges.

Flow variation with angle of attack for the complete configuration.-

The effect of increasing the angle of attack on the complete configuration (fig. 12) resulted in a more complex flow over the canopy than over the 180° canopy alone. The flow over the forward portion of the canopy ahead of the shroud—leading-edge junction points was affected only slightly by the addition of the shrouds and payload; however, the flow over the rearward portion of the canopy behind the shroud attachment points was affected directly by shocks and wakes from the various shrouds, the leading edges, and the payload, plus the interference effects of the combination of these various shocks with the bow shock and any induced separation effects. The effects on the canopy surface flow due to the shroud—leading-edge junction were shown to be substantial by the oil-flow studies, even at  $\alpha = 15^\circ$  near zero lift as well as at all higher angles of attack. At  $\alpha = 15^\circ$ , any flow variations would result only from the combination of the shock waves from the shroud lines and the bow shock and from their effect on the downstream surface flow.

As the angle of attack increased, the flow over the canopy was affected not only by the shrouds but also by the payload so that at  $\alpha = 75^\circ$  there was no area rearward of the shroud-attachment junctions free from relatively high shear. This was substantiated by the results of the temperature-sensitive-paint study which showed that a large percentage of the canopy is subjected to a rate of aerodynamic heating approaching that observed on the nose. The upstream or stagnation side of all shrouds and the spherical payload was also subjected to high heating, whereas the shadow regions were relatively unaffected. This result indicates that the same degree of protection from aerodynamic heating must be provided for all surfaces of a paraglider configuration if it is to be operated over a wide angle-of-attack range at hypersonic speeds.

Reynolds number.- Figure 13 shows the effect of Reynolds number obtained by using temperature-sensitive paint on the complete model and a scaled-up nose section of the complete configuration. The combination of model size and tunnel flow conditions made possible a factor of five in Reynolds number between the two model tests, which were made at an angle of attack of  $30^\circ$ . No clear-cut differences due to Reynolds number were noted although the detail results at the points on the shrouds where the bow shock impinged were more readily ascertained on the larger model. Slight charring of the temperature-sensitive paint occurred at these shock impingement points. This charring indicated that the rate of aerodynamic heating was higher than it was on the stagnation regions on the nose and shrouds, a result that has been noted previously in heat-transfer tests. (See ref. 8.)

## CONCLUSIONS

Analysis of experimental data obtained from wind-tunnel tests on fixed-geometry paraglider configurations at a Mach number of 6.6 and a Reynolds number of  $0.24 \times 10^6$  leads to the following conclusions:

1. Increasing canopy inflation resulted in a general reduction of the lift and drag coefficients throughout most of the test angle-of-attack range, a decrease in maximum lift-drag ratio but an increase in the lift-drag ratio at higher angles of attack, and an increase in the longitudinal stability.

2. The Newtonian theory was generally inadequate for predicting the magnitude of the longitudinal force and moment characteristics for the configurations tested because of the effects of multiple shock waves and the interaction of shock waves from various components. The Newtonian calculations underpredicted all coefficients through the greater portion of the test angle-of-attack range, with the exception of the ratio of lift to drag on the three canopies which was estimated with sufficient accuracy for most engineering needs. Estimates of pitching moment were fair in the low and medium angle-of-attack range.

3. The interference-flow regions on the canopy produced by adding the shrouds and payload to the fully inflated canopy significantly increased the loading on the canopy. This resulted in an increase in the lift and drag coefficients throughout the test angle-of-attack range and a decrease of the lift-drag ratio in the medium angle-of-attack region. The maximum lift-drag ratio of the canopy alone was reduced from 1.53 to 1.05 by the addition of shrouds and payload. The effects of adding shrouds and payload were inadequately predicted because these important interference effects are not accounted for by Newtonian theory.

4. Regions or spots of high shear as indicated by the oil-flow technique were shown to be areas exposed to a high aerodynamic heating rate, compared with the heating rate on the nose, by use of temperature-sensitive-paint tests.

5. Temperature-sensitive-paint studies indicated that the addition of shrouds and payload to the canopy severely aggravated the aerodynamic heating, particularly in the vicinity of the shroud-leading-edge intersection and the regions of shock and wake impingement on the canopy downstream of the shrouds. It appears that the same degree of protection from aerodynamic heating must be provided for all portions of the paraglider configuration before hypersonic operation is feasible.

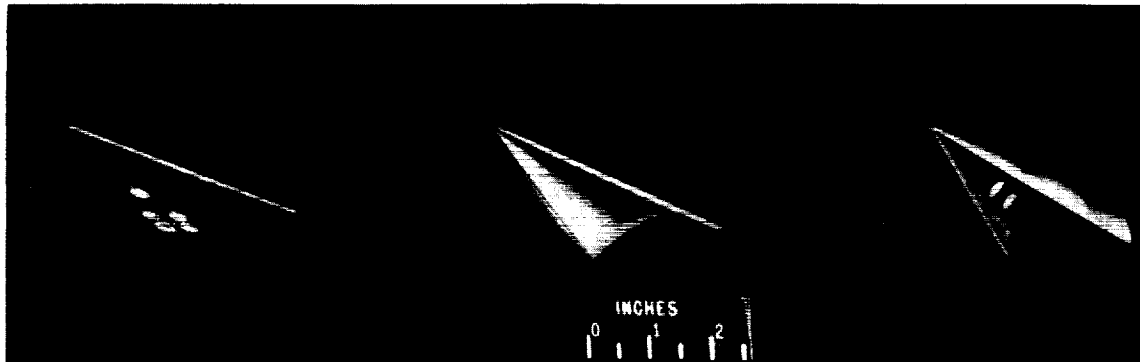
L  
1  
8  
4  
9

6. There appeared to be no variation in the regions of aerodynamic heating on the paraglider configuration as a result of increasing the Reynolds number by a factor of five.

Langley Research Center,  
National Aeronautics and Space Administration,  
Langley Air Force Base, Va., December 4, 1961.

#### REFERENCES

1. Rogallo, F. M., and Lowry, J. G.: Flexible Reentry Gliders. Preprint No. 175C, Soc. Automotive Eng., Apr. 1960.
2. Rogallo, Francis M., Lowry, John G., Croom, Delwin R., and Taylor, Robert T.: Preliminary Investigation of a Paraglider. NASA TN D-443, 1960.
3. Naeseth, Rodger L.: An Exploratory Study of a Parawing as a High-Lift Device for Aircraft. NASA TN D-629, 1960.
4. Hewes, Donald E.: Free-Flight Investigation of Radio-Controlled Models With Parawings. NASA TN D-927, 1961.
5. Grimmering, G., Williams, E. P., and Young, G. B. W.: Lift on Inclined Bodies of Revolution in Hypersonic Flow. Jour. Aero. Sci., vol. 17, no. 11, Nov. 1950, pp. 675-690.
6. Rainey, Robert W.: Working Charts for Rapid Prediction of Force and Pressure Coefficients on Arbitrary Bodies of Revolution by Use of Newtonian Concepts. NASA TN D-176, 1959.
7. Pender, Harold, McIlwain, Knox, eds.: Electrical Engineers' Handbook - Electric Communication and Electronics. Third ed., John Wiley & Sons, Inc., 1945, pp. 1-14 - 1-15.
8. Newlander, Robert A.: Effect of Shock Impingement on the Distribution of Heat-Transfer Coefficients on a Right Circular Cylinder at Mach Numbers of 2.65, 3.51, and 4.44. NASA TN D-642, 1961.

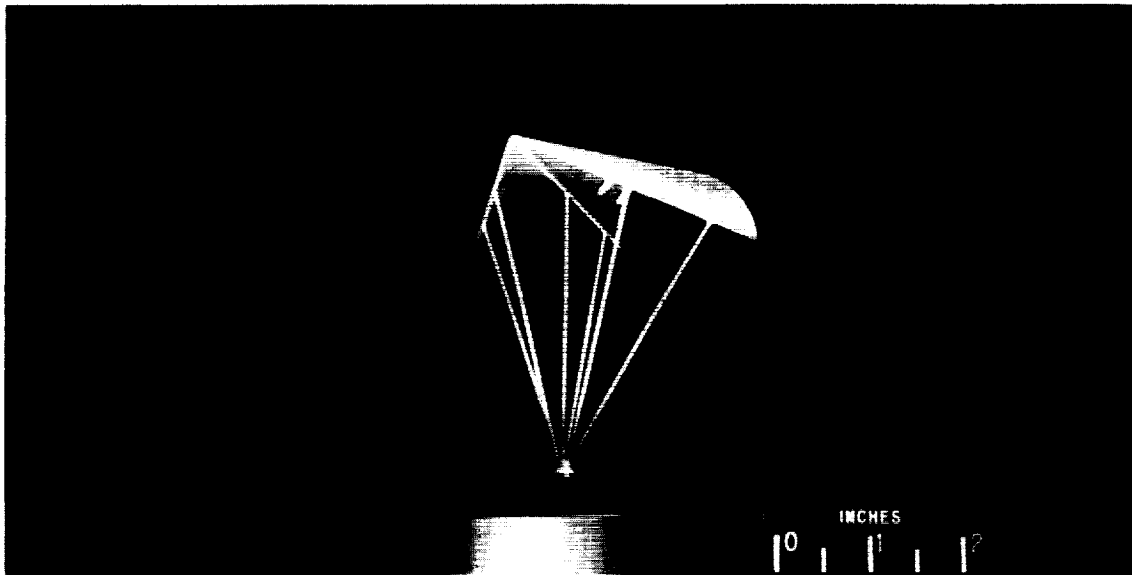


0° canopy

100° canopy

180° canopy

(a) Parawing configurations.

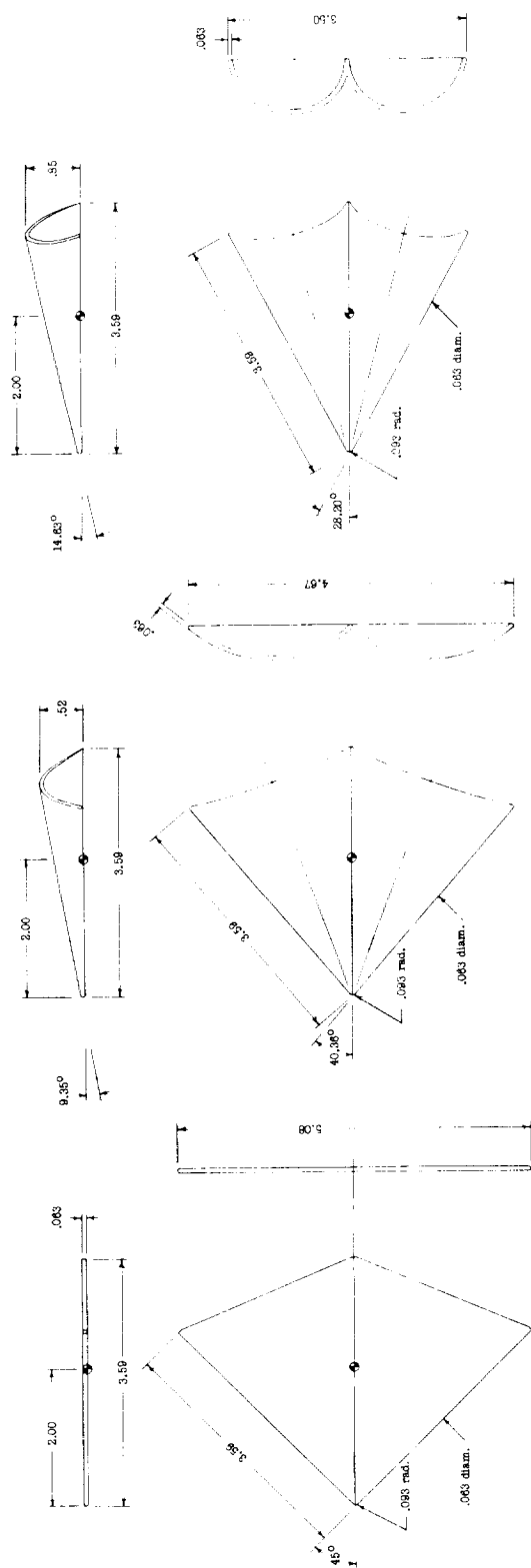


(b) Complete paraglider configuration.

L-61-8070

Figure 1.- Photographs of steel force models used in investigation.

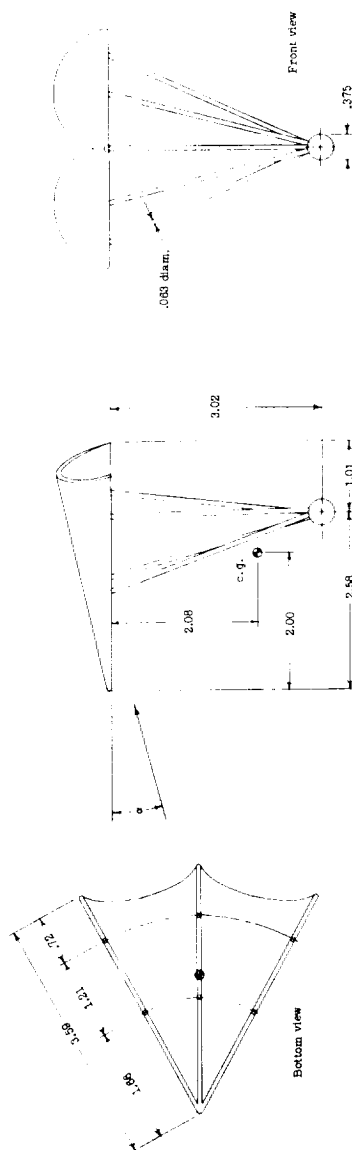
L-1849



(a) 0° canopy.

(b) 100° canopy.

(c) 180° canopy.



(d) Complete paraglider configuration.

Figure 2.- Detail drawing of force models. All dimensions are in inches.

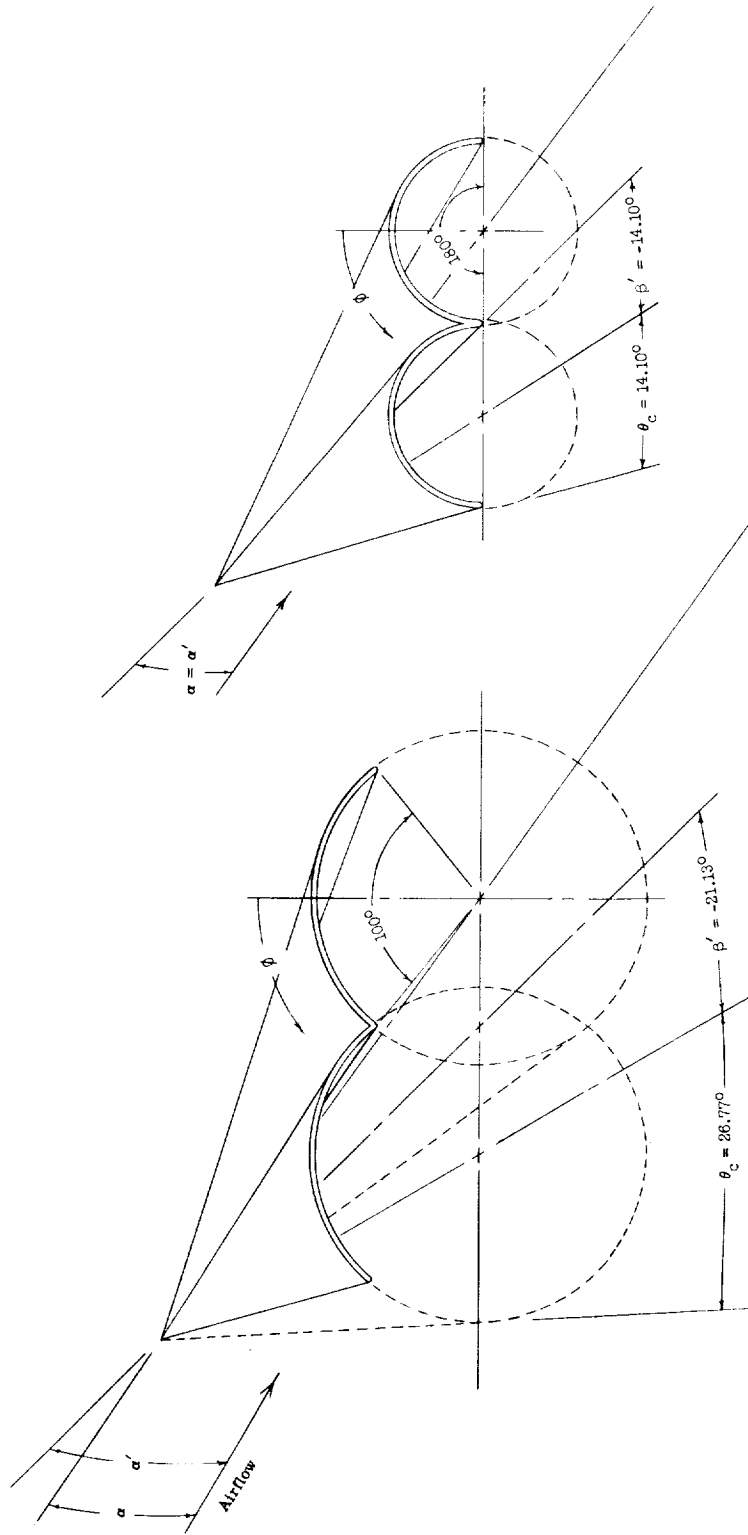
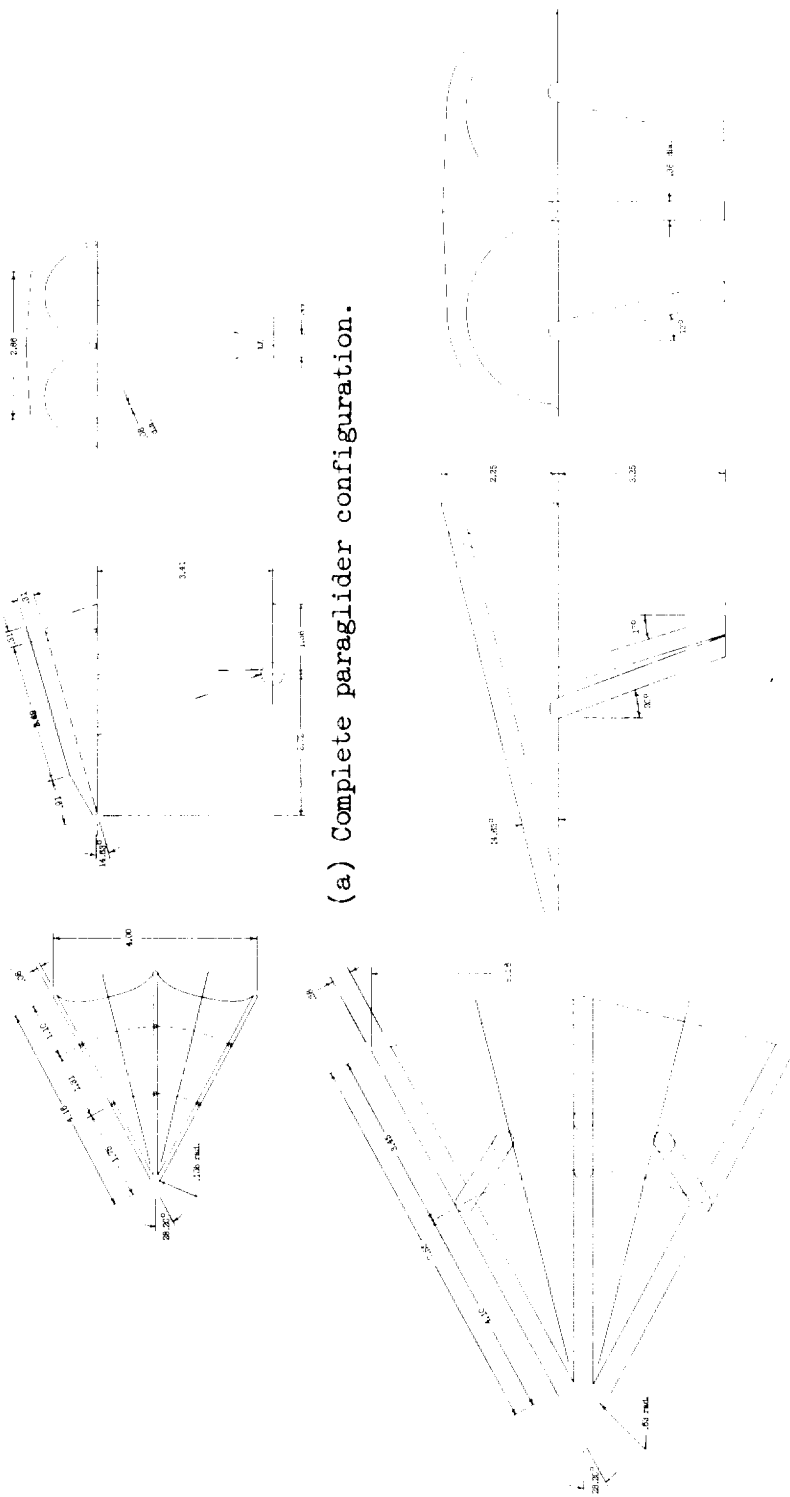
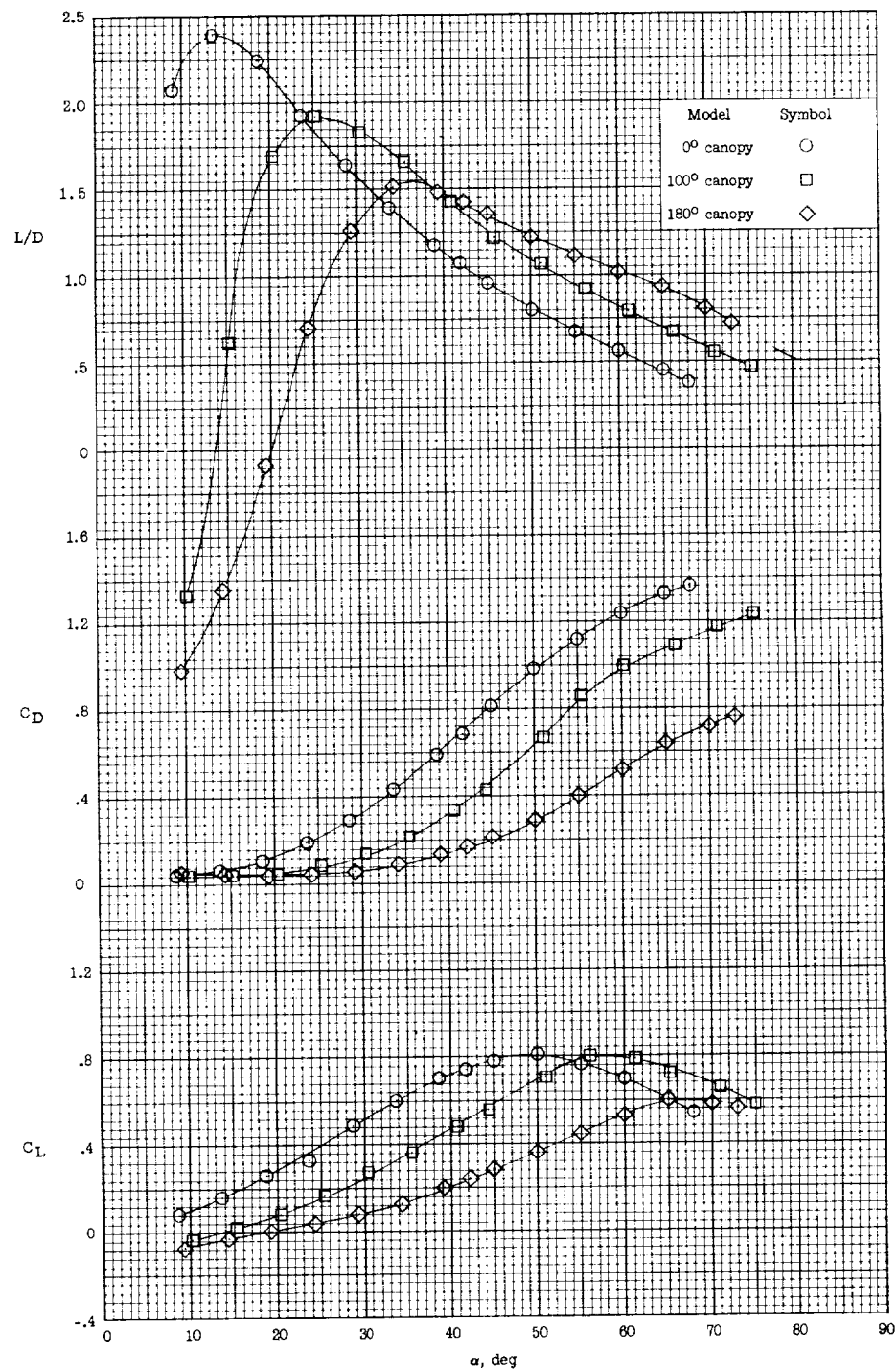


Figure 3.- Schematic drawing showing development of surfaces and notation used for calculations.



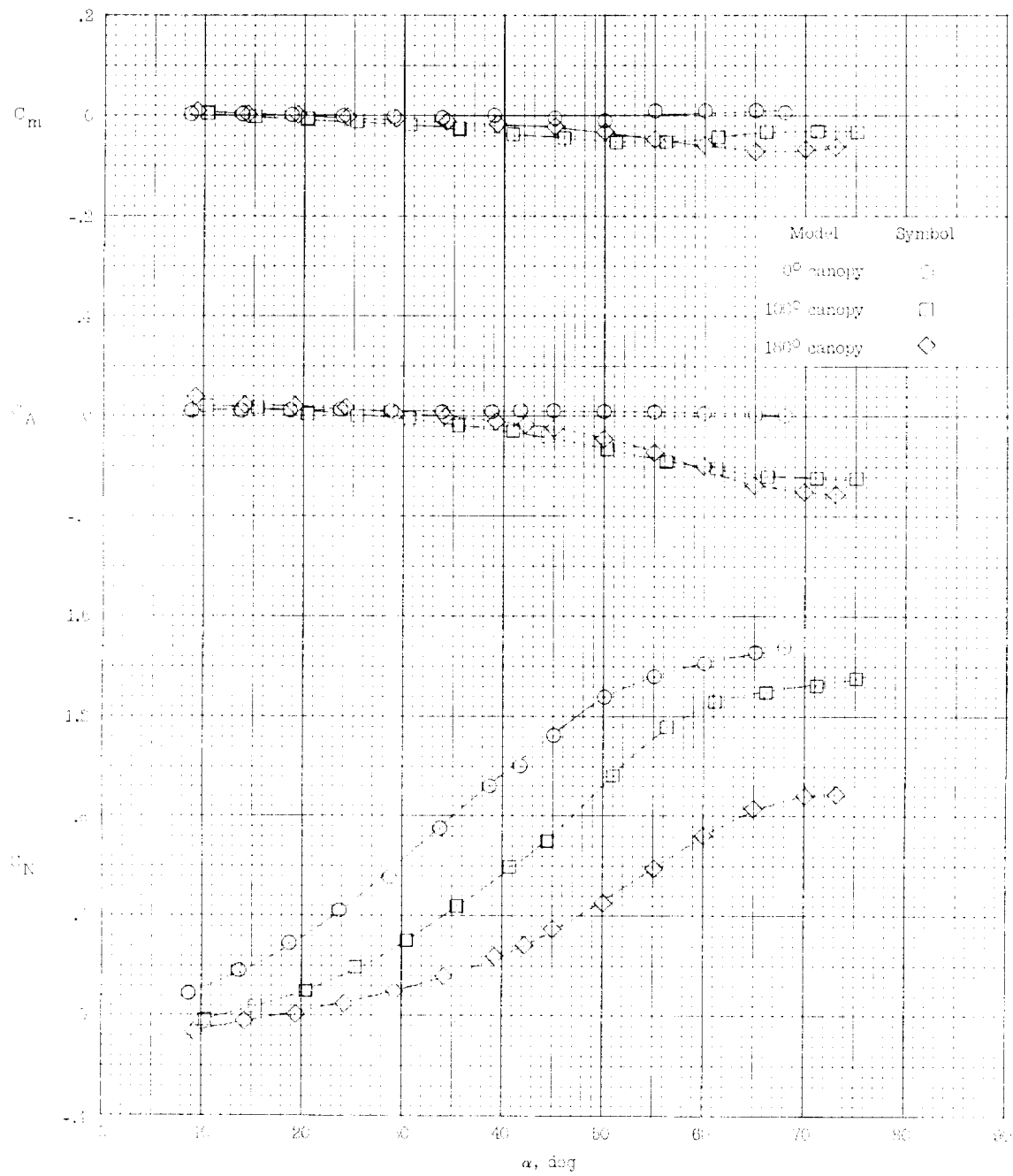
(b) Enlarged nose section of complete paraglider configuration.

Figure 4.- Detail drawing of models used for temperature-sensitive-paint tests. All dimensions are in inches.



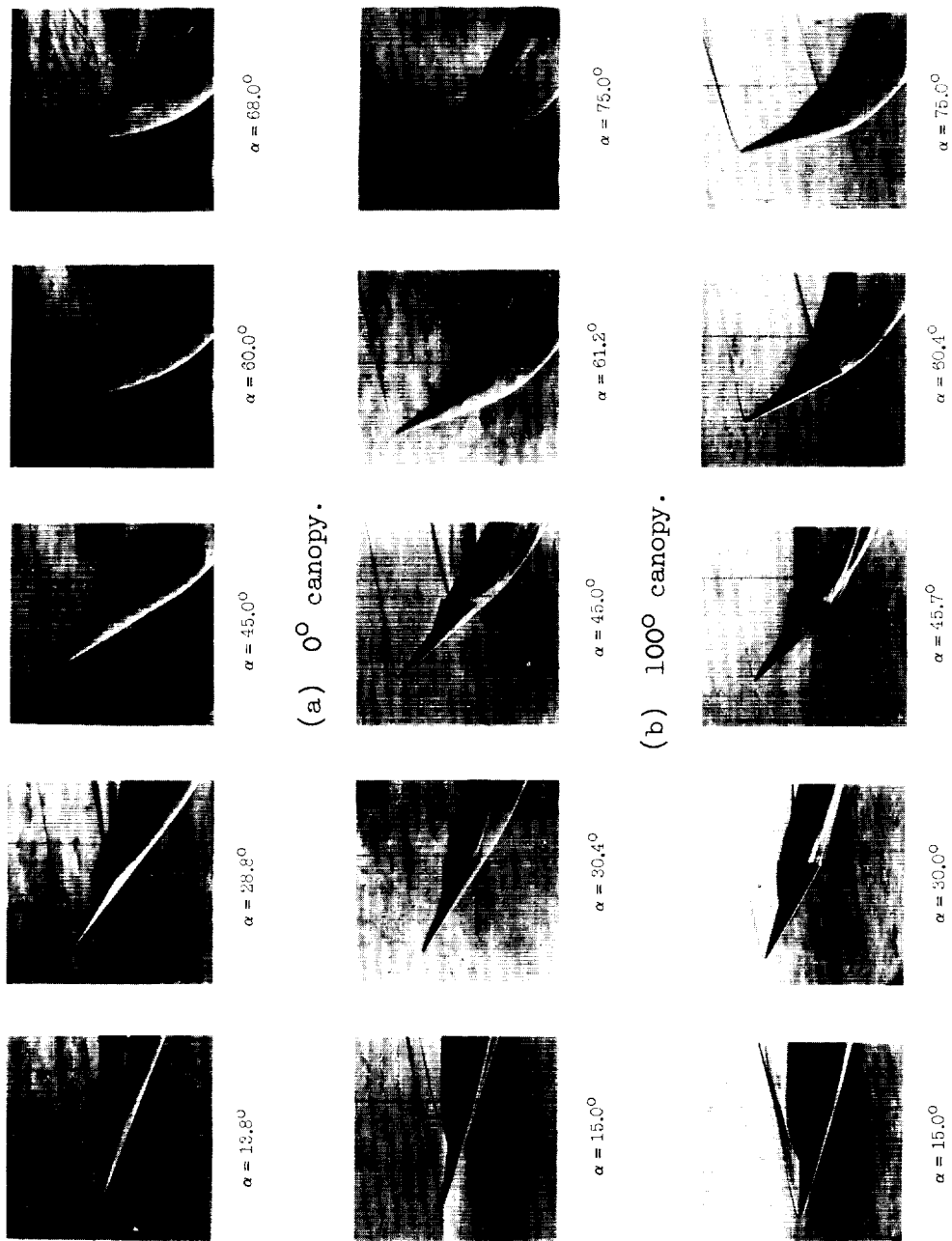
(a) Lift, drag, and lift-drag ratio.

Figure 5.- Effect of the degree of canopy inflation on longitudinal characteristics of paraglider canopy.  $M_\infty = 6.6$ ;  $R_\infty = 0.24 \times 10^6$ .



(b) Normal force, axial force, and pitching moment.

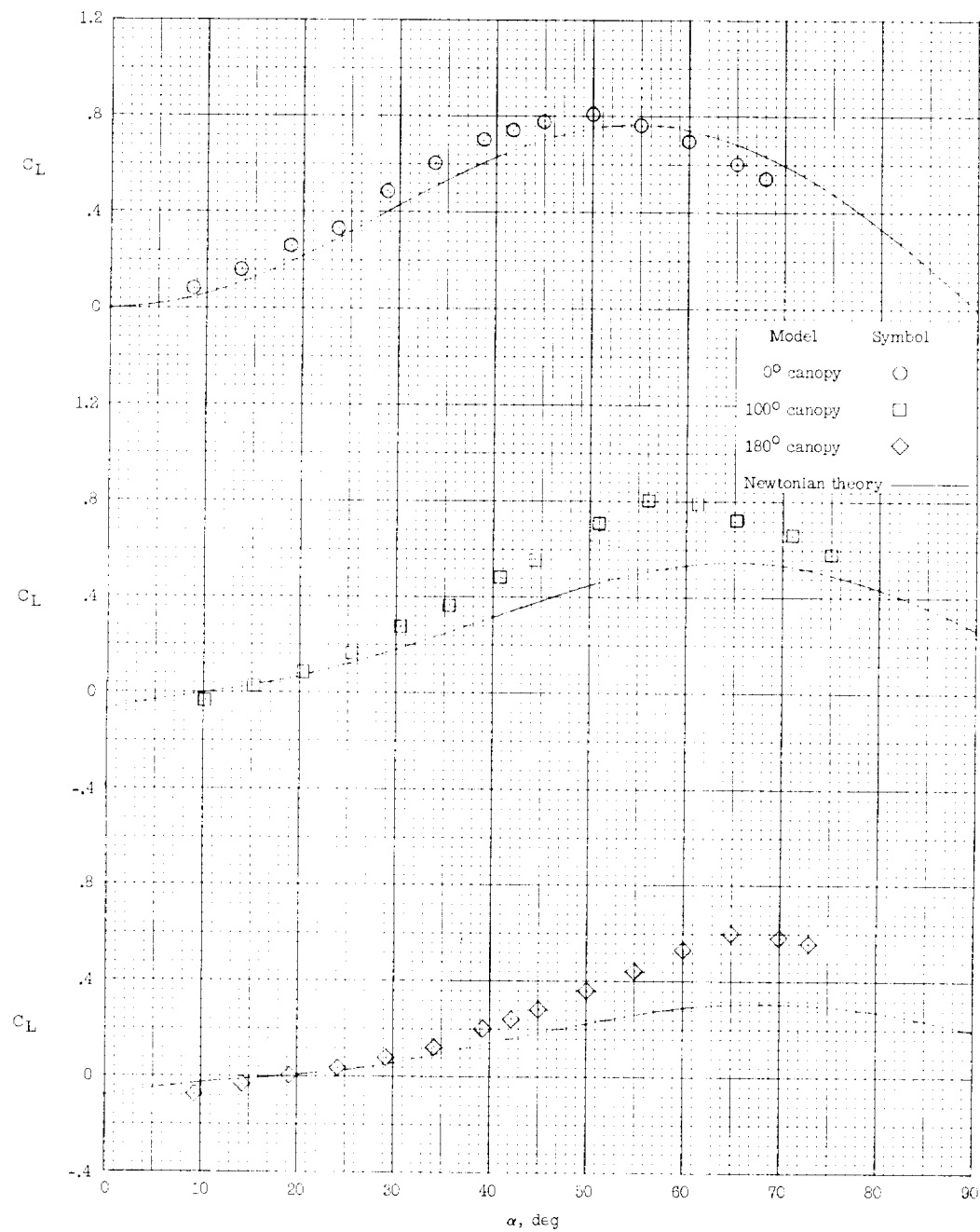
Figure 5.- Concluded.



L-61-8401

(c)  $180^\circ$  canopy.Figure 6.- Schlieren photographs of various canopies.  $M_\infty = 6.6$ ;  $R_\infty = 0.24 \times 10^6$ .

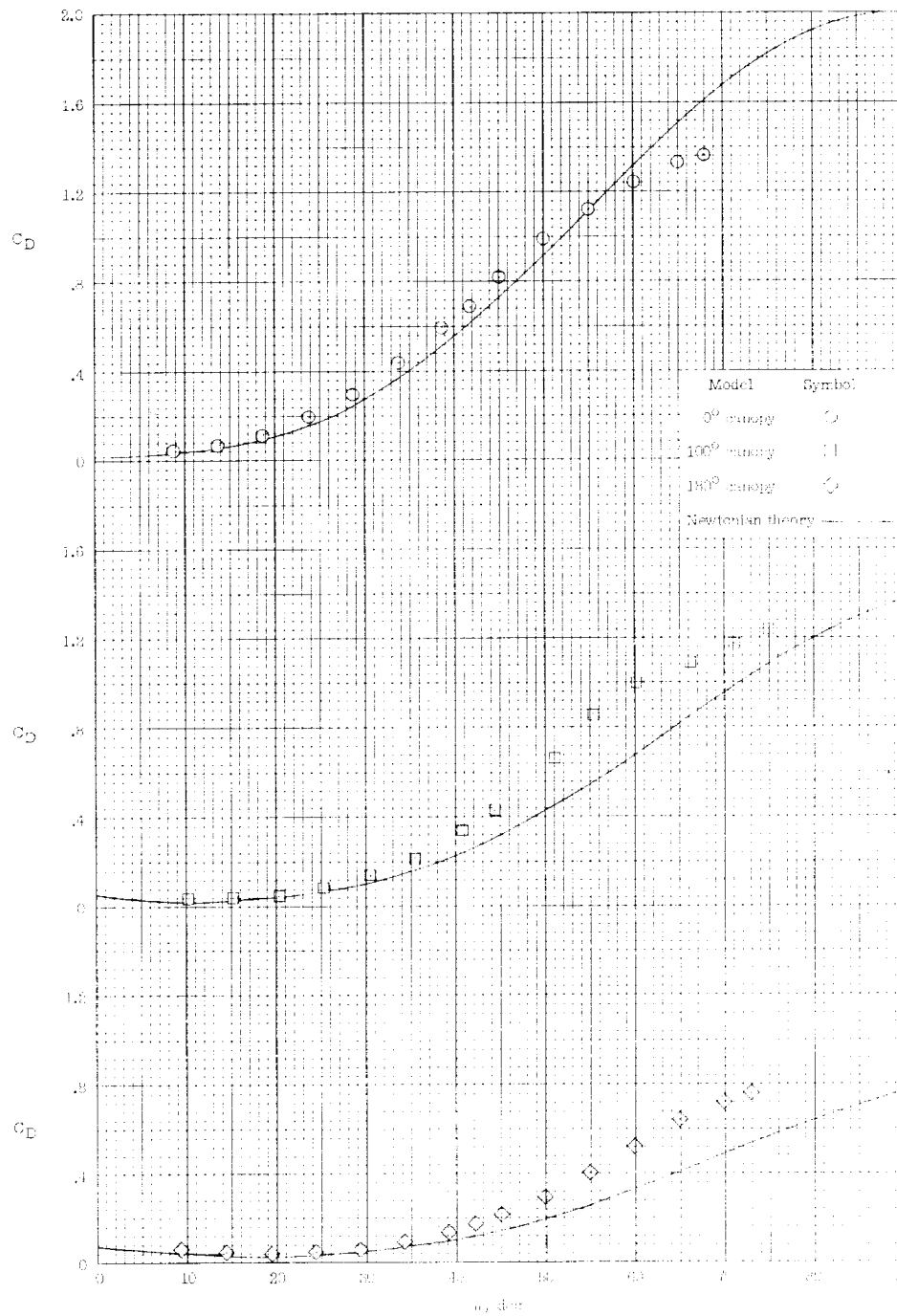
L-1849



(a) Lift.

Figure 7.- Comparison of longitudinal characteristics of three canopies of various degrees of canopy inflation with Newtonian theory.

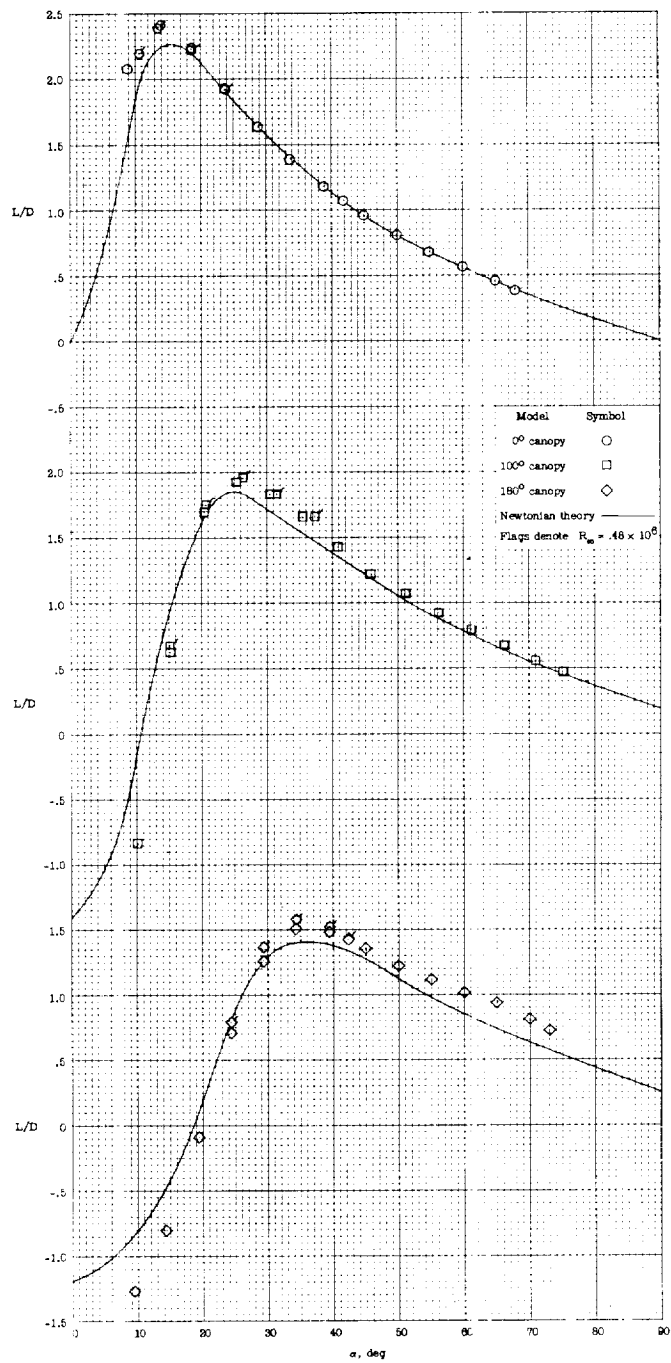
$$M_\infty = 6.6; R_\infty = 0.24 \times 10^6.$$



(b) Drag.

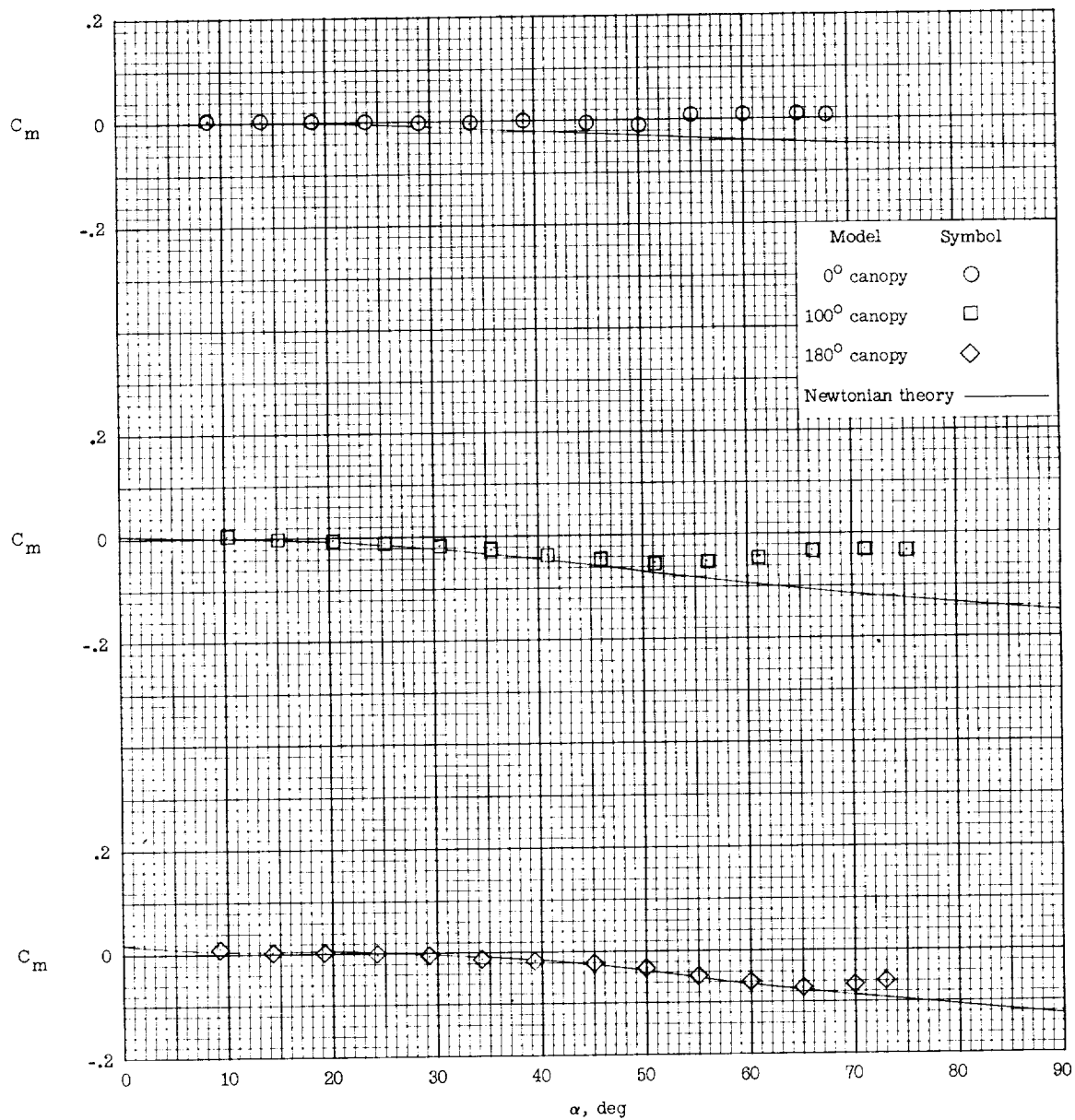
Figure 7.- Continued.

L-1849



(c) Lift-drag ratio.

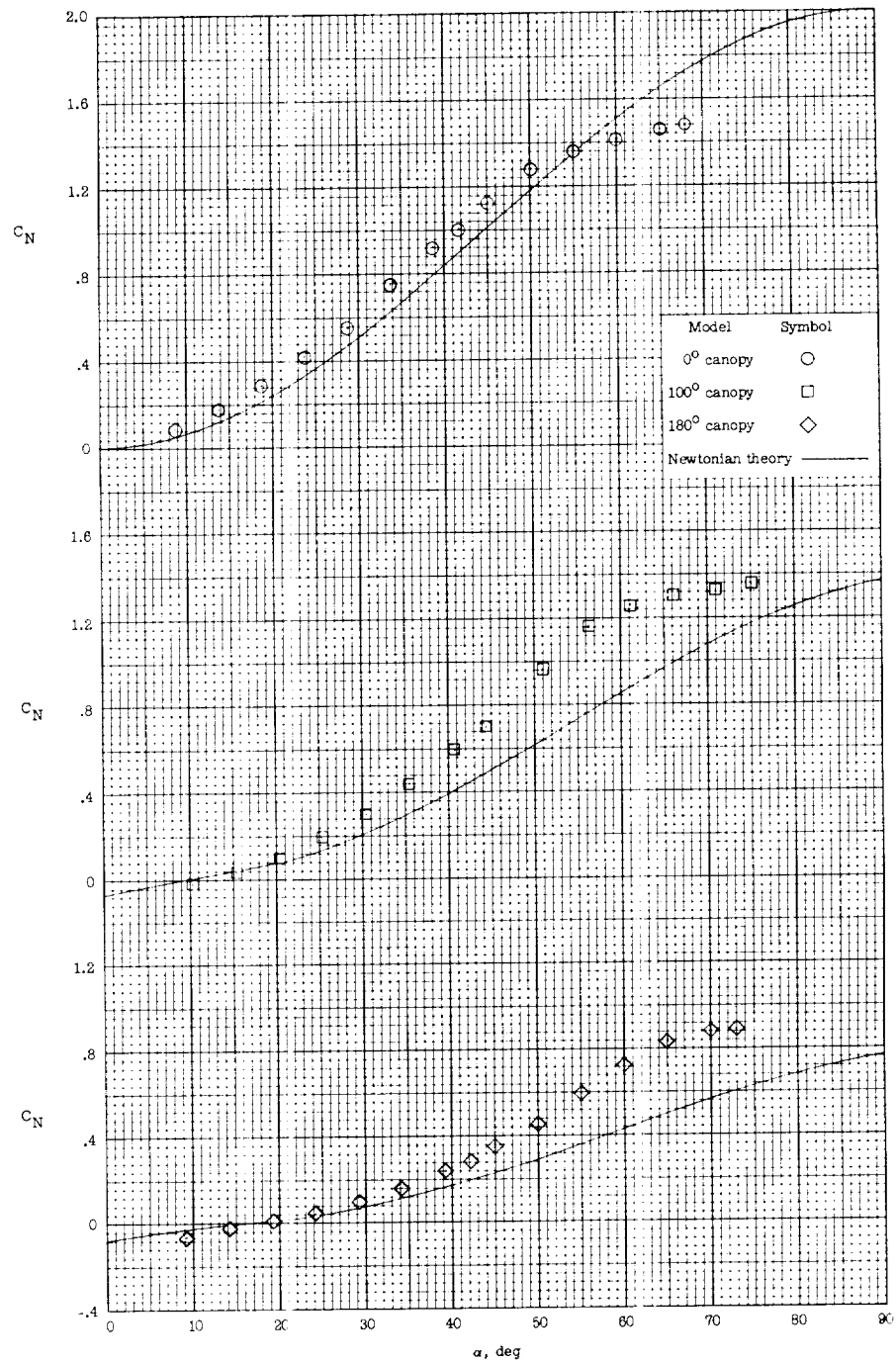
Figure 7.- Continued.



(d) Pitching moment.

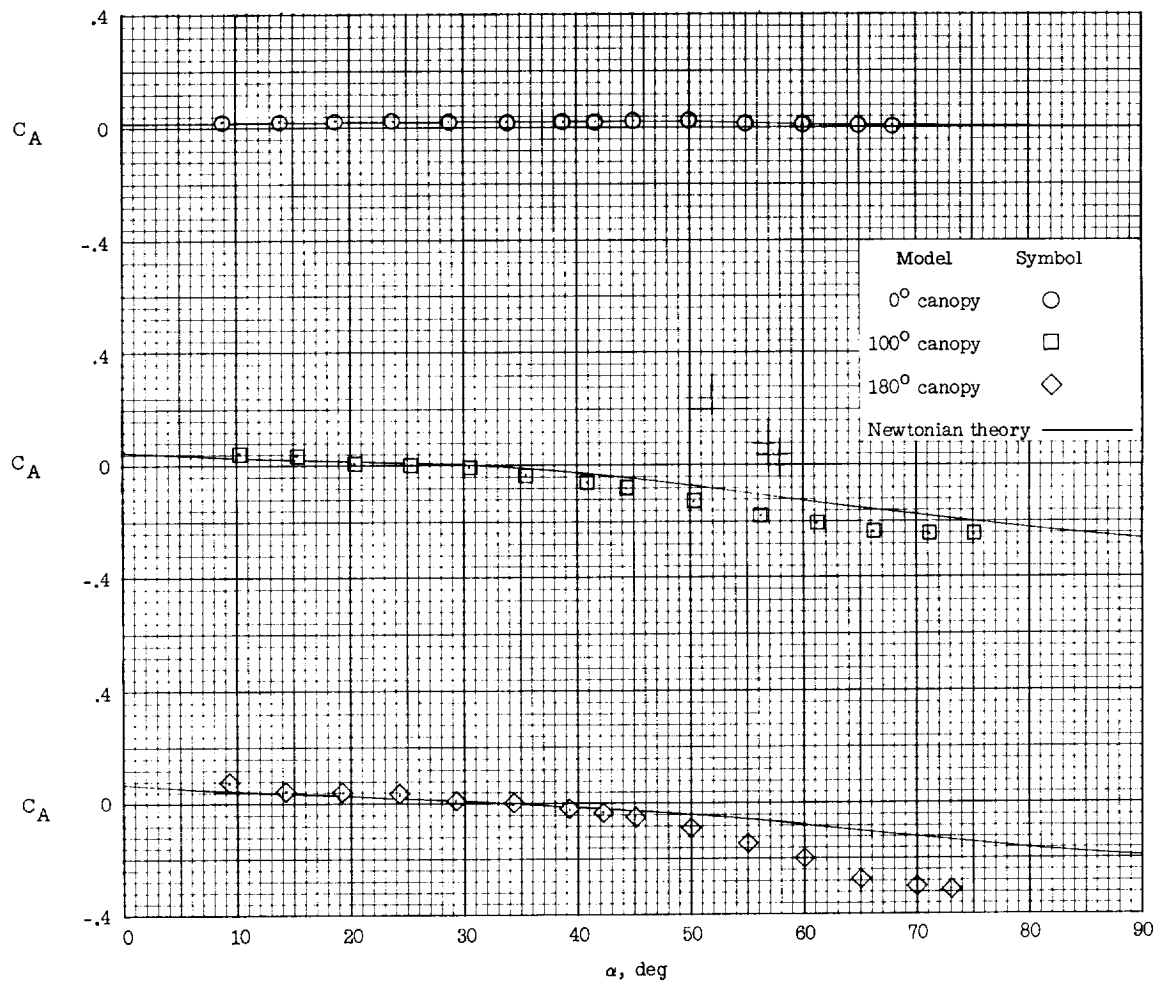
Figure 7.- Continued.

L-1849



(e) Normal force.

Figure 7.- Continued.



(f) Axial force.

Figure 7.- Concluded.

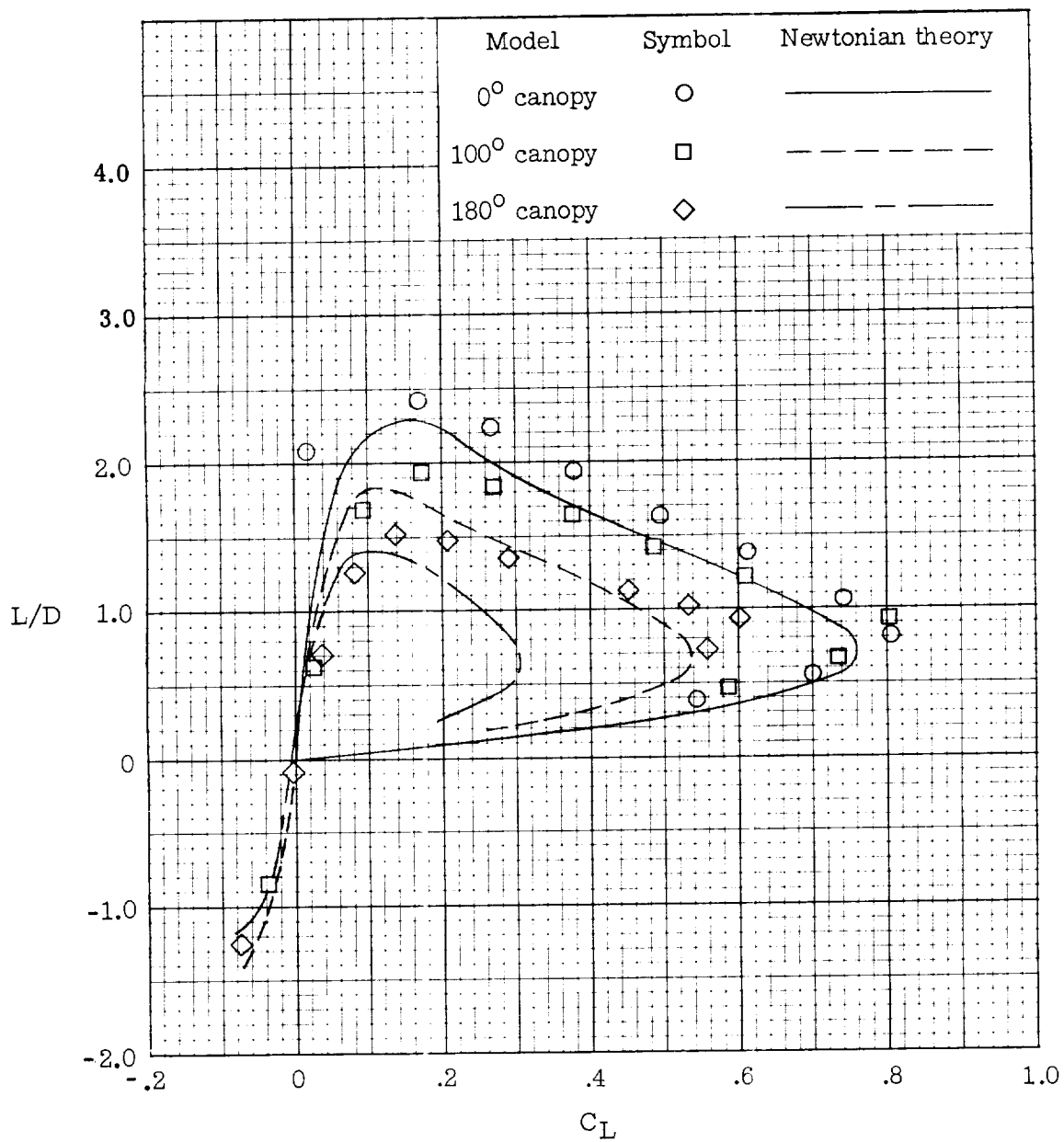
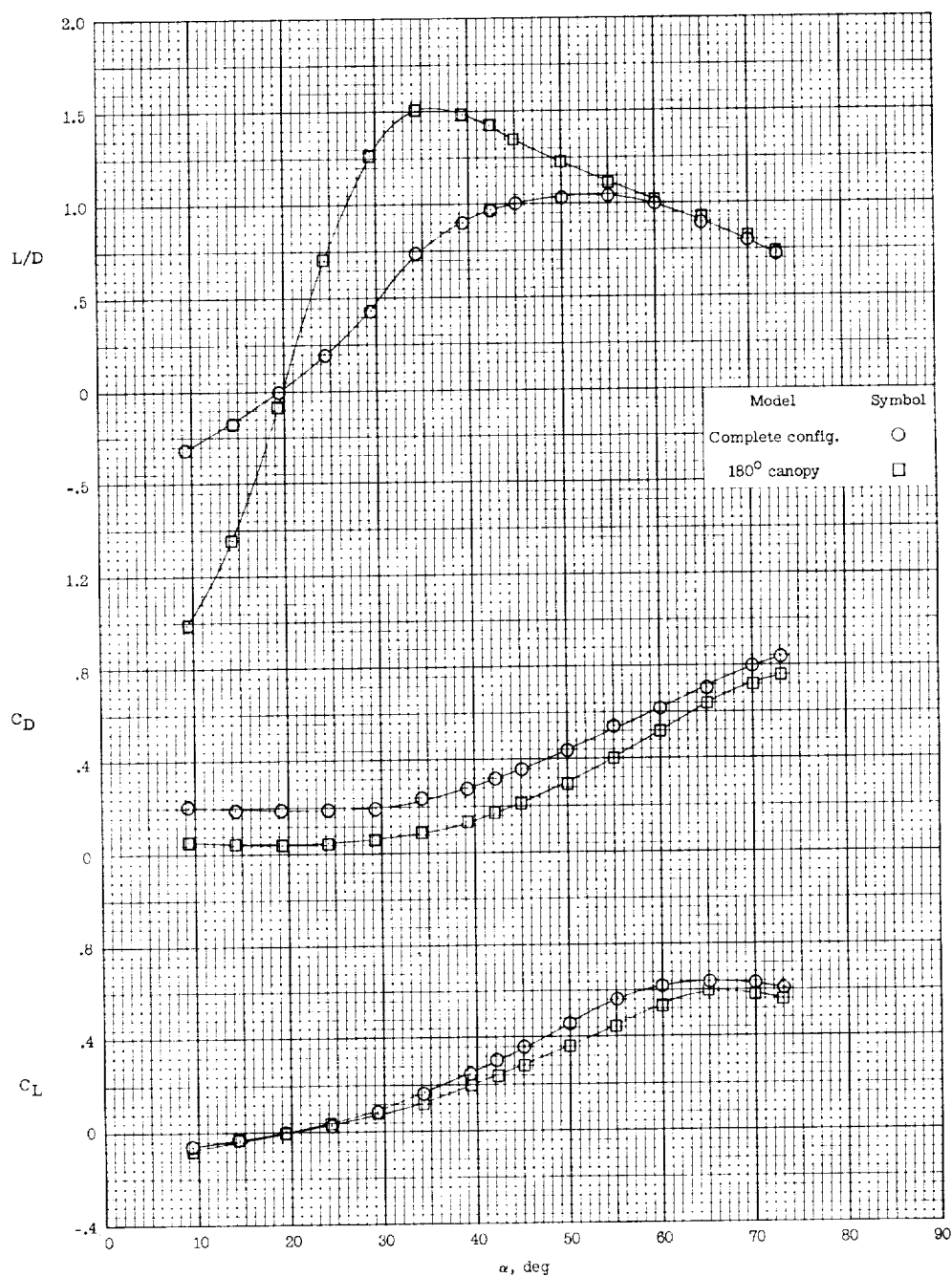
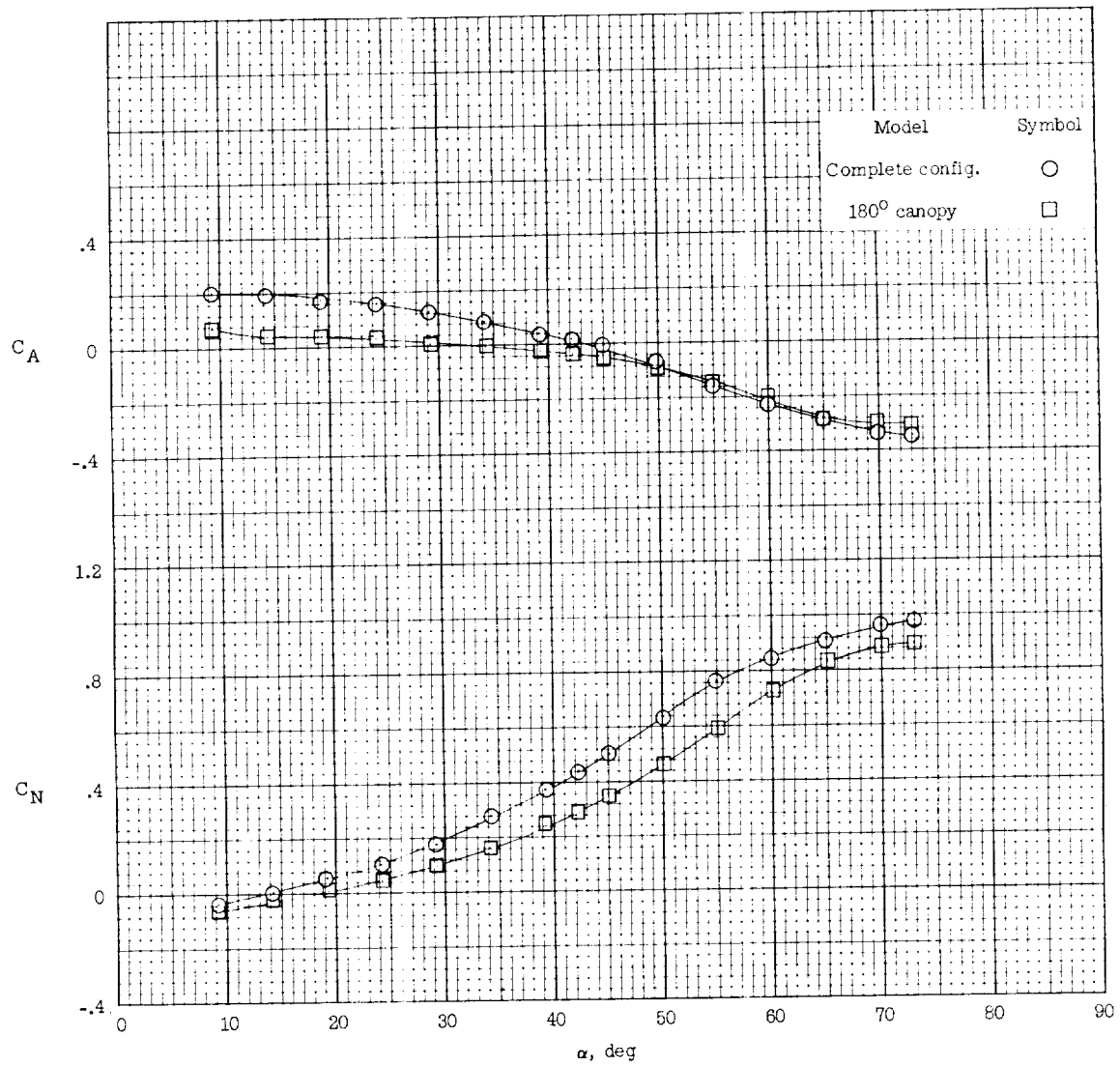


Figure 8.- Comparison of lift-drag ratios and lift coefficients of various canopies.  $M_\infty = 6.6$ ;  $R_\infty = 0.24 \times 10^6$ .



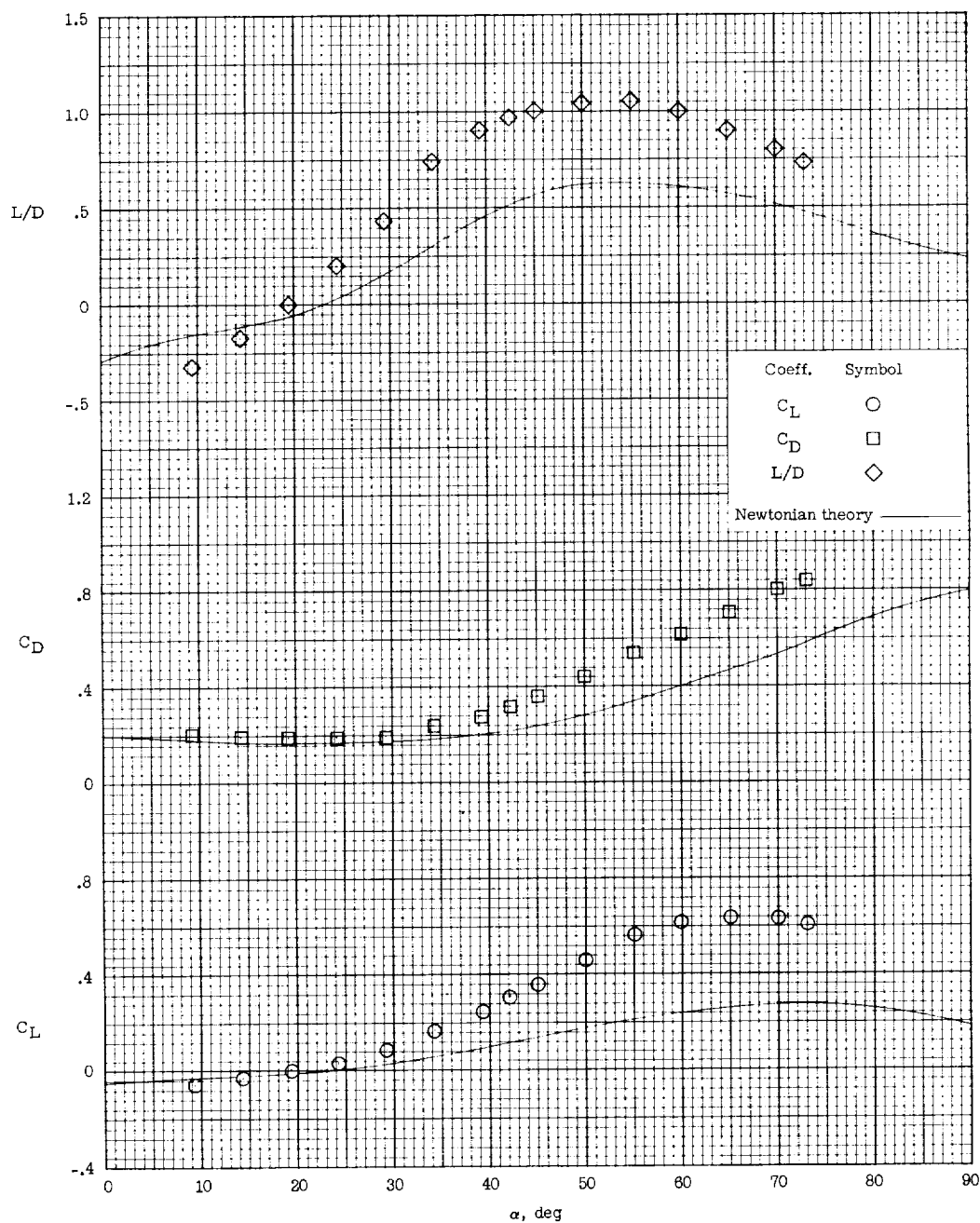
(a) Lift, drag, and lift-drag ratio.

Figure 9.- Effect of addition of shrouds and payload on longitudinal characteristics of 180° canopy.  $M_\infty = 6.6$ ;  $R_\infty = 0.24 \times 10^6$ .



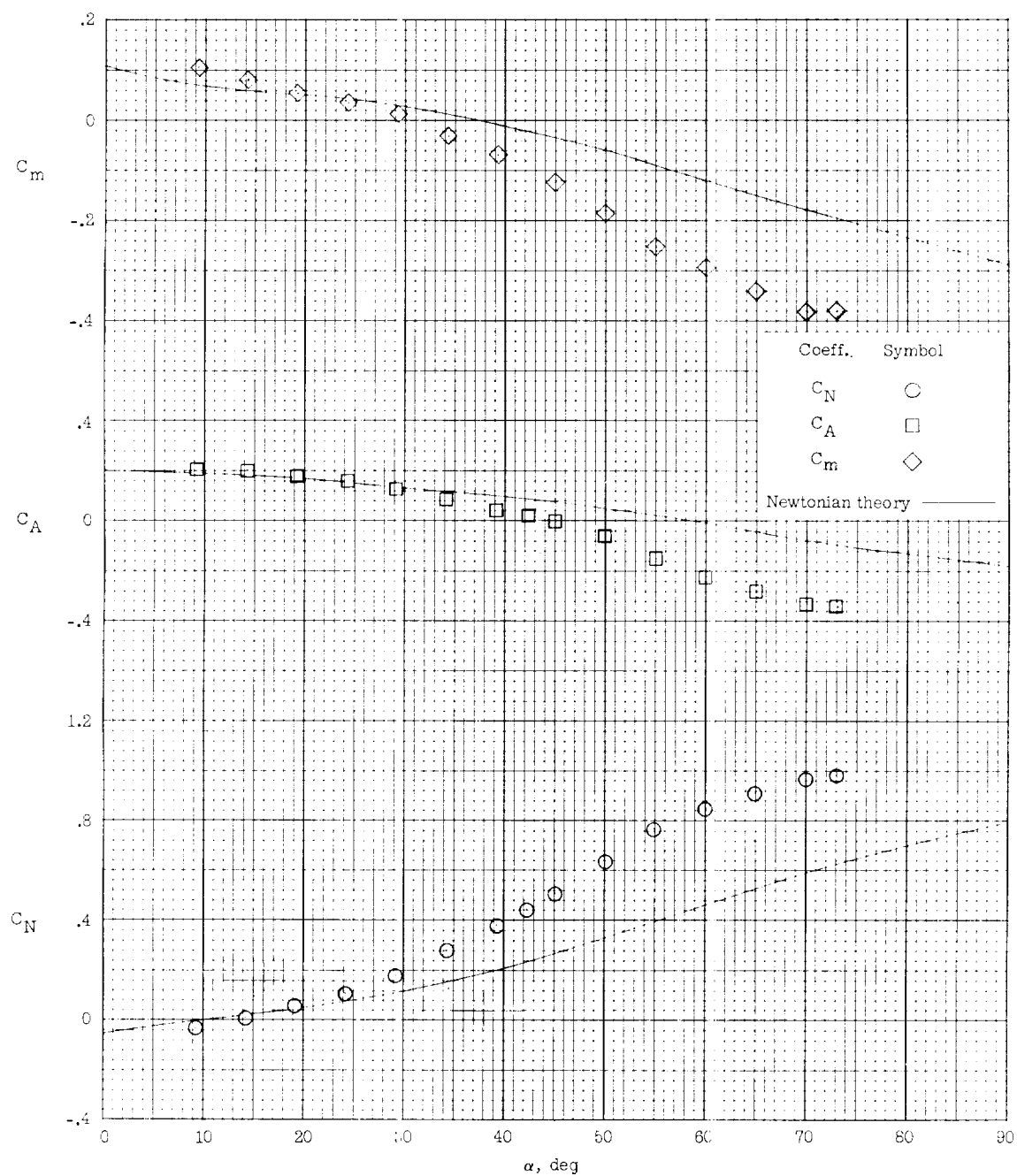
(b) Normal force and axial force.

Figure 9.- Concluded.



(a) Lift, drag, and lift-drag ratio.

Figure 10.- Comparison of longitudinal characteristics of complete paraglider configuration with Newtonian theory.  $M_\infty = 6.6$ ;  
 $R_\infty = 0.24 \times 10^6$ .

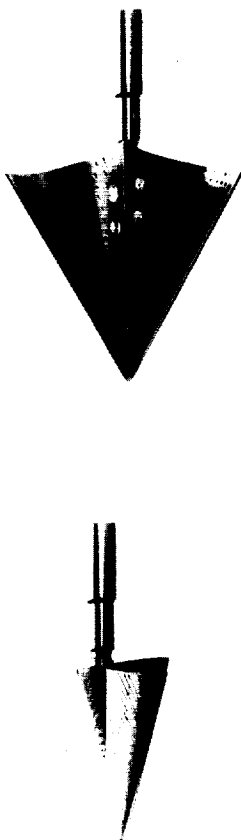


(b) Normal force, axial force, and pitching moment.

Figure 10.- Concluded.



Schlieren

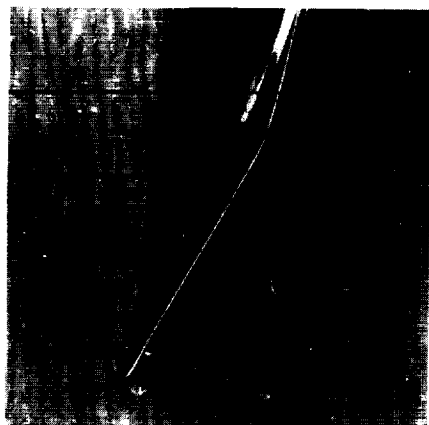


Oil flow

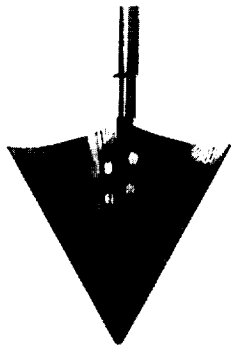
(a)  $\alpha = 15^\circ$ .

L-61-8071

Figure 11.- Comparison of photographs of schlieren, oil flow, and temperature-sensitive-paint investigations of  $180^\circ$  canopy configuration at various angles of attack.  $M_\infty = 6.6$ ;  $R_\infty = 0.24 \times 10^6$ .



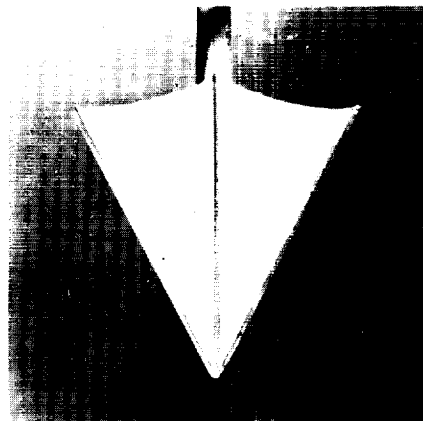
Schlieren



Oil flow



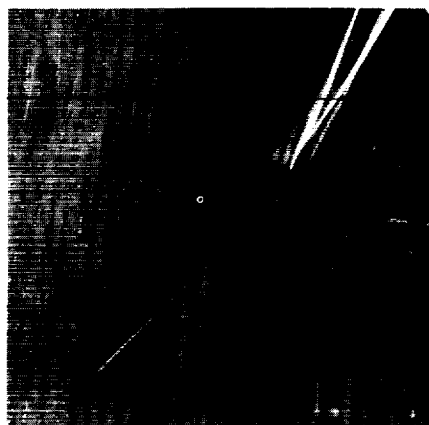
Temperature-sensitive paint



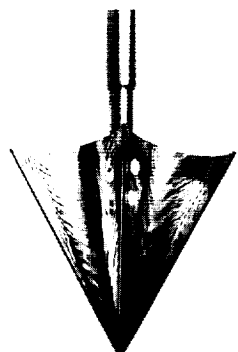
(b)  $\alpha = 30^\circ$ .

L-61-8072

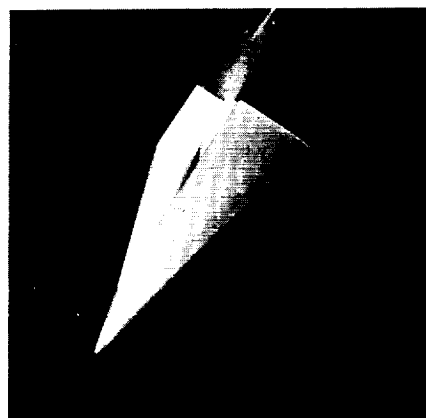
Figure 11.- Continued.



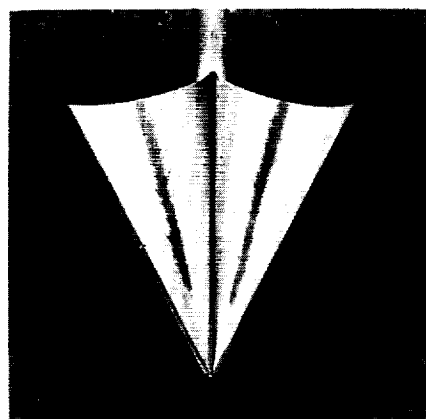
Schlieren



Oil flow



Temperature-sensitive paint



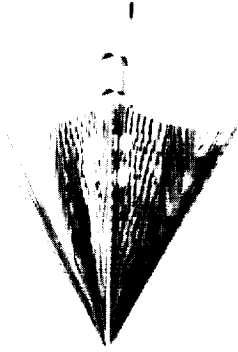
(c)  $\alpha = 45^\circ$ .

Figure 11.- Continued.

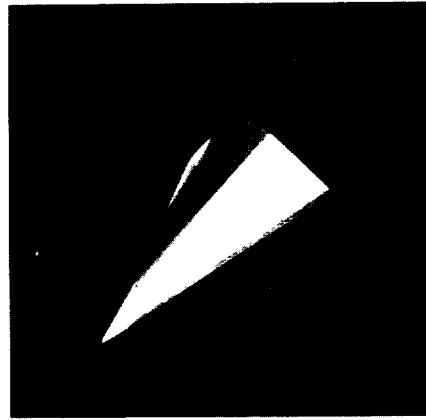
L-61-8073



Schlieren



Oil flow

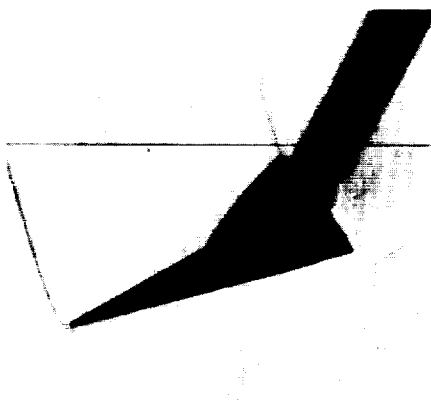


Temperature-sensitive paint

(d)  $\alpha = 60^\circ$ .

L-61-8074

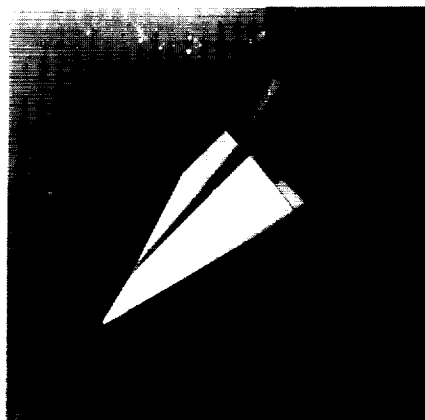
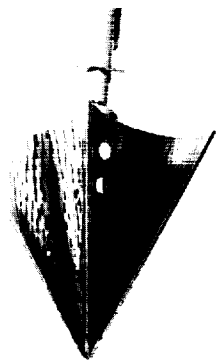
Figure 11.- Continued.



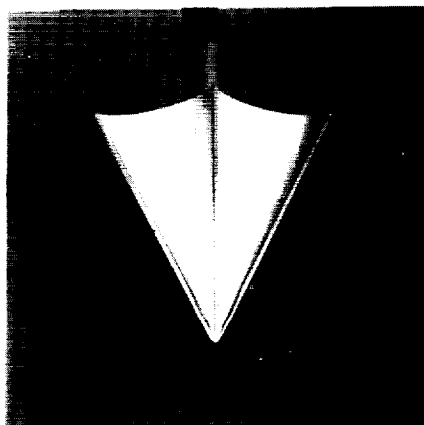
Schlieren



Oil flow



Temperature-sensitive paint



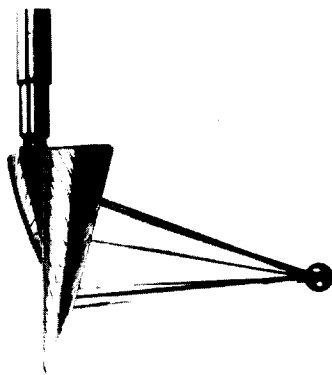
(e)  $\alpha = 75^\circ$ .

L-61-8075

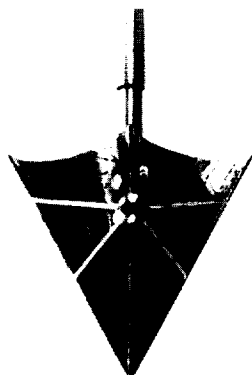
Figure 11.- Concluded.



Schlieren



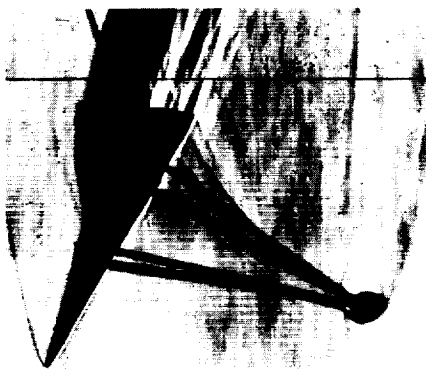
Oil flow



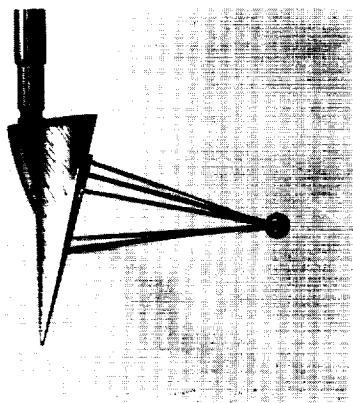
(a)  $\alpha = 15^\circ$ .

L-61-8402

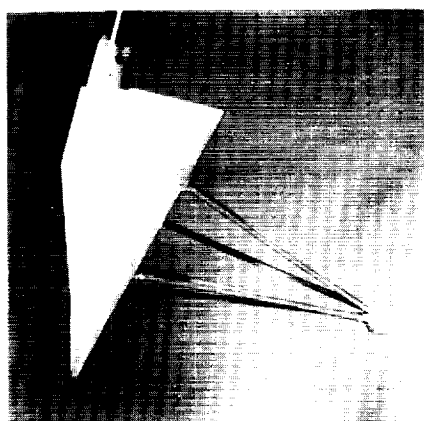
Figure 12.- Comparison of photographs of schlieren, oil flow, and temperature-sensitive-paint investigations of complete paraglider configuration at various angles of attack.  $M_\infty = 6.6$ ;  $R_\infty = 0.24 \times 10^6$ .



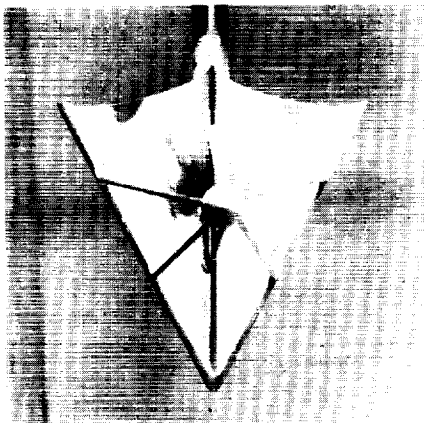
Schlieren



Oil flow



Temperature-sensitive paint

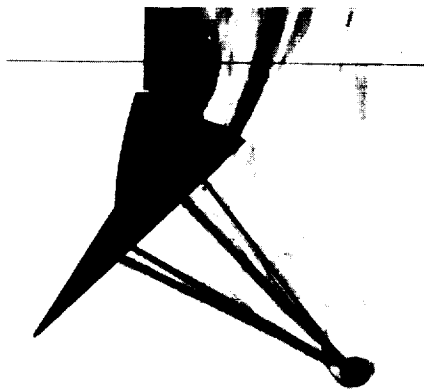


(b)  $\alpha = 30^\circ$ .

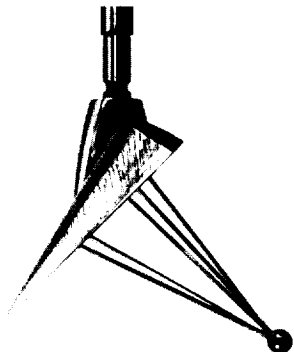
L-61-8403

Figure 12.- Continued.

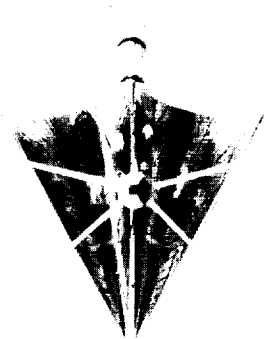
L-1849



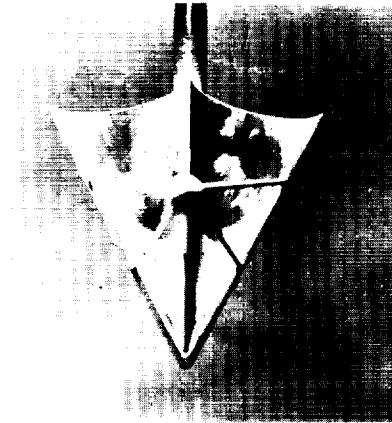
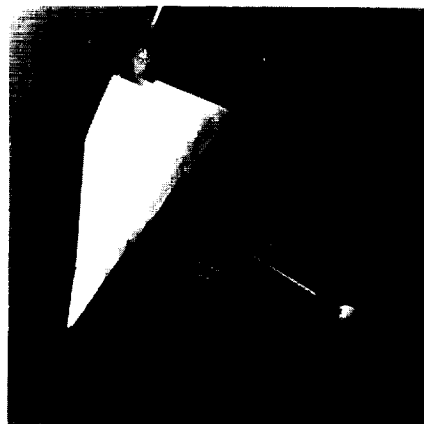
Schlieren



Oil flow



Temperature-sensitive paint



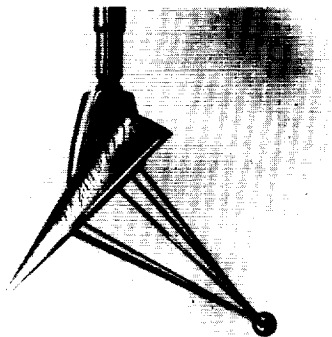
(c)  $\alpha = 45^\circ$ .

Figure 12.- Continued.

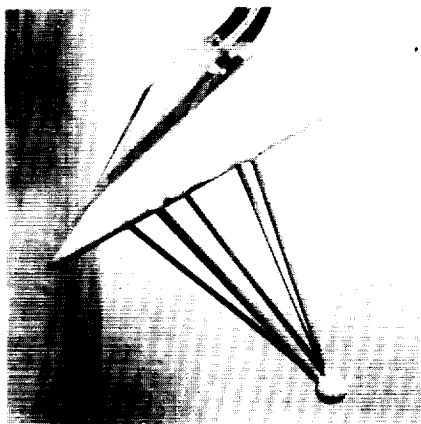
L-61-8404



Schlieren



Oil flow



Temperature-sensitive paint

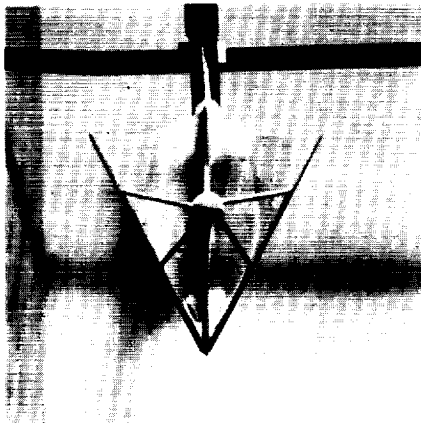
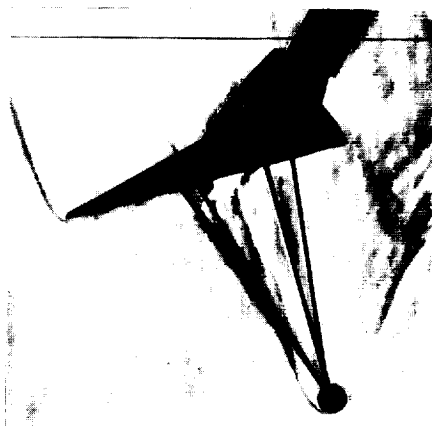
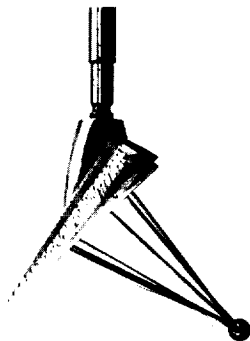
(d)  $\alpha = 60^\circ$ .

Figure 12.- Continued.

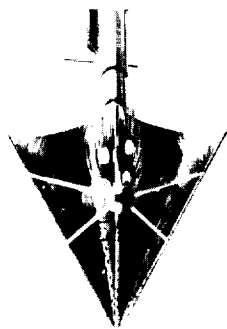
L-61-8405



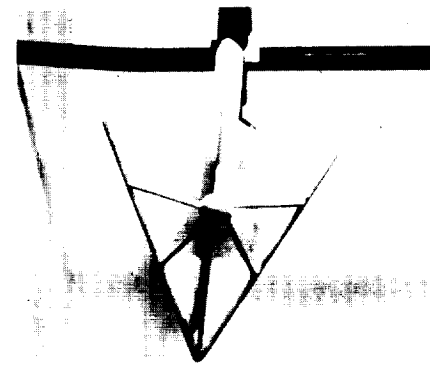
Schlieren



Oil flow



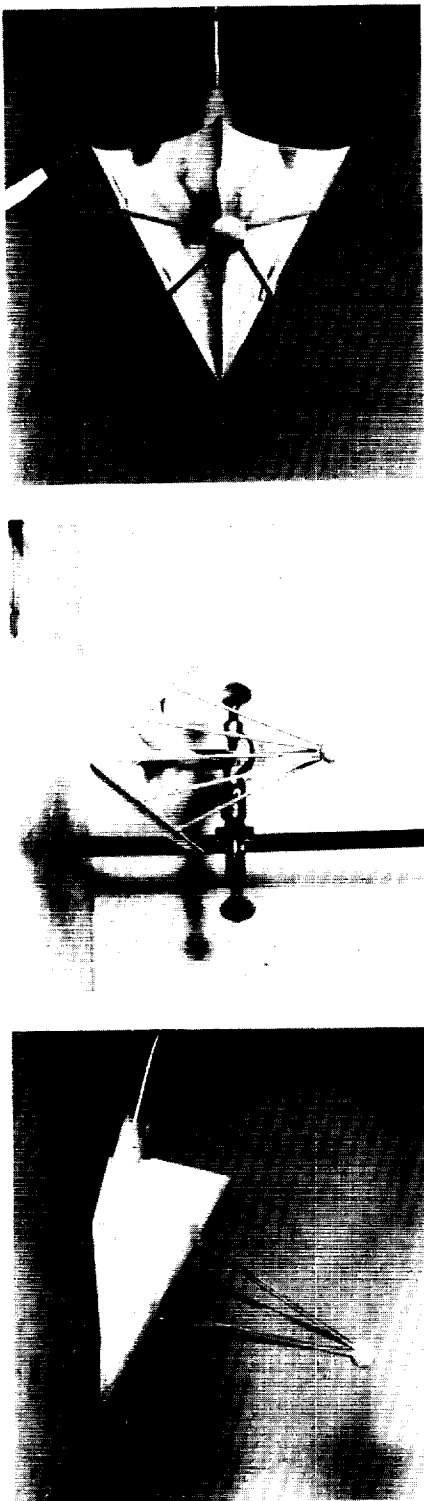
Temperature-sensitive paint



(e)  $\alpha = 75^\circ$ .

L-61-8406

Figure 12.- Concluded.



(a) Complete paraglider configuration.  $R_{\infty} = 0.24 \times 10^6$ .



(b) Enlarged nose section of complete paraglider configuration.  $R_{\infty} = 1.2 \times 10^6$ .

Figure 13.- Effect of Reynolds number on aerodynamic heating characteristics of complete paraglider configuration ( $180^\circ$  canopy) in vicinity of leading-edge—shroud intersection by means of temperature-sensitive-paint tests.  $M_{\infty} = 6.6$ ;  $\alpha = 30^\circ$ .